applied sciences

MDPI

Article

The Potential of Focusing Acoustic Retroreflectors for Architectural Surface Treatment

Densil Cabrera [1,*], Shuai Lu [1,2], Jonothan Holmes [1] and Manuj Yadav [1,3]

[1] Sydney School of Architecture, Design and Planning, The University of Sydney, Sydney, NSW 2006, Australia
[2] Tsinghua Shenzhen International Graduate School, Shenzhen 518055, China
[3] Institute for Hearing Technology and Acoustics, RWTH Aachen University, Kopernikusstr. 5, 52074 Aachen, Germany
* Correspondence: densil.cabrera@sydney.edu.au

Featured Application: The concepts developed in this paper could be used in buildings to increase acoustic comfort in rooms for speech. Such treatments could play a role in increasing local acoustic support for talkers in rooms without relying on diffuse reverberation. Possible contexts for indoor application include didactic rooms (e.g., classrooms) and multi-talker rooms (e.g., offices, eating establishments)—with potential benefits including increased speaking comfort, reduced voice strain, reduced distraction from irrelevant speech, and reduced multi-talker speech build-up.

Abstract: How much sound can a building surface reflect to a source, the location of which is not exactly known? This paper considers this question particularly for a planar surface acting as an array of retroreflectors, or of focusing retroreflectors. The question is investigated using finite-difference time-domain acoustic simulation, using ideal retroreflective patches achieved by space-reversal, and focusing achieved by delays. Extensive (7.2 × 7.2 m) and local (2.4 × 2.4 m) ideal planar reflector arrays were investigated at distances of 1.5 to 4 m from sources that were within a 2.4 × 2.4 m square plane. Patch sizes ranged from 0.3 m squares to the full reflector size. Physically realizable non-ideal focusing retroreflectors based on parabolic trihedra were also investigated. With sufficiently large patches, ideal focusing retroreflector arrays consistently outperform non-focusing retroreflector arrays. A large focusing retroreflector array has the potential to provide retroreflected energy levels (speech and A-weighted) from the first reflection to a source at 2 m distance comparable to the diffuse field energy level of acoustically supportive reverberant rooms. A small focusing retroreflector array returns less sound, but still much more than a single reflection from an equivalent specularly reflecting surface. Results from parabolic trihedra demonstrate that retroreflected energy levels similar to those from ideal surfaces can be achieved by architectural form. Challenges in translating these concepts to practical design solutions are discussed.

Keywords: room acoustics; architectural acoustics; sound reflection; retroreflection; focusing retroreflector; acoustic focusing; voice support; FDTD

Citation: Cabrera, D.; Lu, S.; Holmes, J.; Yadav, M. The Potential of Focusing Acoustic Retroreflectors for Architectural Surface Treatment. *Appl. Sci.* **2023**, *13*, 1547. https://doi.org/10.3390/app13031547

Academic Editor: Edoardo Piana

Received: 31 December 2022
Revised: 21 January 2023
Accepted: 22 January 2023
Published: 25 January 2023

1. Introduction

Sound reflection in rooms, when designed well, can make a substantial contribution to acoustic quality. For some types of room, sound reflected back to the source—a talker or musician—can be beneficial. This is well-established in auditorium acoustics for music, where the stage support parameters indicate aspects of the acoustic quality for performers [1–4]. In rooms for speech, reflections back to the talker can often be beneficial, leading to a more comfortable environment for talking and affecting the characteristics of speech [5–8]. Straightforward approaches to increasing reflected sound returned to a talker include using directed or local reflections and relying on reverberation. However,

those approaches have limitations: directed/local reflections rely on a designer knowing where the talker(s) will be; and reverberation has hazards of reduced intelligibility and noise build-up in rooms. This paper explores the possibility of providing strong acoustic reflections back to a talker, without knowledge of the talker's position, and without relying on reverberation. The concept introduced is arrays of focusing acoustic retroreflectors, which are shown, in principle, to potentially provide reflected sound energy comparable to that of the reverberation of a supportive room.

The voice regulation phenomenon of reduced vocal output caused by greater electroacoustic support is sometimes known as 'sidetone compensation' [8,9], but has also been called the 'room effect' to signify the role of support from room reflections [6,10]. It is closely related to the better-known Lombard effect [11], whereby people instinctively raise their voices in the presence of background noise—both can be explained by a talker instinctively maintaining the audibility of their own voice [9,12,13]. However, the extent of these effects depends on the communication scenario/task [14–17] (e.g., reading to oneself, holding a conversation, lecturing, etc.), and voice regulation is affected by multimodal perception [18].

Benefits of acoustic support for talkers have been investigated in particular for teachers. Sustained speech by teachers using high levels of projection is associated with voice strain and discomfort [19]. Classrooms with somewhat greater acoustic support have been shown to lead to reduced voice projection [6,20], especially for teachers who experience voice strain [21], but limited to a workable reverberation time [22]. Hence, although generally established intelligibility-oriented recommendations are for reverberation time in the vicinity of 0.4 s or less [23], a field study by Puglisi et al. [22] found 0.7 s to provide optimum acoustic support; and Pelegrín-García et al. [24] propose similar recommendations, noting that some national classroom recommendations include relatively long reverberation times appropriate for acoustic support of teachers.

Room types other than classrooms also could potentially benefit from strong acoustic support for talkers. Multi-talker spaces could be candidates, considering that a reduction in each person's acoustic power would reduce babble noise build-up—this problem has been studied particularly in large public rooms and eating establishments [25–32]. In work environments such as open-plan offices, speech distraction from irrelevant intelligible speech is a widespread problem [33–37]. In such contexts, reflecting a talker's sound back to them might not only have a voice regulation effect, but also ameliorate unwanted transmission to others, potentially improving the masking of unwanted speech by ambient sound. Another possible context is outdoor areas, which typically have very little acoustic support unless near buildings. Some studies have investigated open air environments using room acoustics concepts [38–41], and certain outdoor activities might benefit from enhanced acoustic support whilst preserving their openness.

This paper leaves the development and assessment of such applications to future studies. Before considering how a didactic or multi-talker room could be better served by acoustically supporting talkers, the basic question of what can be achieved by acoustic reflectors needs to be answered. Hence, the main concern of this paper is how much sound *could* be reflected back to a talker from the first reflection.

1.1. Theoretical Perspectives on Reflected Sound Level

1.1.1. Reflected Sound Level from a Single Reflection

The sound returned to a source by a single reflection from an extensive flat hard surface can be simply estimated from Equation (1), where $r_{\min}$ is the minimum distance from source to the surface (normal incidence), and the result is expressed relative to the emitted sound at 1 m. For example, a surface 2 m from the source yields −12 dB, which is independent of frequency.

$$L_{\text{retro}} = -20\log(2r_{\min}) \quad (1)$$

For a finite surface, the reflected sound calculation can also account for diffraction (Equation (2)). Diffraction coefficient D is frequency-dependent, and is approximately

calculated via Equation (3) (limited to the simple case of a square reflector in free space with edge lengths $l_x = l_y$ and the source-receiver in line with its centroid), where λ is wavelength, and FresnelC and FresnelS are cosine and sine Fresnel integrals, respectively [42]. For a large surface with a collocated source-receiver in line with the surface's centroid and within a few meters from it, $D \approx 1$ over the speech frequency range. However, diffraction losses become substantial at low frequencies if small or distant surfaces subtending a small solid angle are considered. Furthermore, diffraction has a ripple response that may boost the reflected sound in parts of the spectrum.

$$\frac{p^2_{\text{retro}}}{p^2_{1\text{m}}} = \frac{D}{4r^2_{\text{min}}} \tag{2}$$

$$D = 2\left(\text{FresnelC}\left(\frac{l_x}{\sqrt{\lambda r_{\text{min}}}}\right)^2 + \text{FresnelS}\left(\frac{l_x}{\sqrt{\lambda r_{\text{min}}}}\right)^2\right) \tag{3}$$

The maximum possible sound returned to a source from a single reflection can be calculated by considering a source at the center of a large perfectly reflecting sphere. The reflected pressure at the focus can be expressed via Equation (4) [43]. The squared pressure increases with squared wave number (k), i.e., at 6 dB/octave. When considering the first reflection only, the size of the sphere does not affect the pressure magnitude, assuming the sphere is sufficiently large. Theta is the angle over which a spherical cap covers ($0 \leq \vartheta \leq \pi$), with π representing the complete sphere.

$$\frac{p^2_{\text{focus}}}{p^2_{1\text{m}}} = p^2_{1\text{m}} k^2 (1 - \cos\vartheta)^2 \tag{4}$$

Analyses in this paper are evaluated using combined omnidirectional speech-weighting and A-weighting (Section 2.1.3), for which the maximum sound at the focus from Equation (4) is 32.7 dB ($\vartheta = \pi$) relative to the emitted sound pressure level at 1 m (calculated over the 125 Hz–8 kHz octave bands). For a hemisphere ($\vartheta = \pi/2$), the sound returned to the focus is 26.6 dB.

Another ideal scenario could be that emitted sound is returned to the source, but incoherently. This ideal can be evaluated by energetically summing the sound that the surface is exposed to, leading to a simple frequency-independent relationship with the surface's solid angle, Ω (Equation (5)).

$$L_{\text{retro}} = 10\log(\Omega/4) \tag{5}$$

If all emitted sound is energetically summed, the result is 5 dB (for $\Omega = 4\pi$ steradians) relative to the emitted sound at 1 m; or 2 dB for an extensive ceiling ($\Omega = 2\pi$). Cabrera et al. [44] observed that this simple concept was reasonably good as a predictor of measured retroreflection from building façades comprised of arrays of concave trihedral corners. This equation conservatively points to the potential of retroreflective surface treatments (such as of ceilings), yielding values much greater than a specular surface (when surfaces are extensive), but much less than a coherent focusing surface.

1.1.2. Reflected Sound Level from Room Reverberation

Classical room acoustics theory provides another important perspective on the potential sound returned to a source, using the assumption of a diffuse field. This approach neglects particular reflections, and instead integrates the whole reverberant sound energy over time, assuming that it is spatially invariant. Relative to the emitted sound at 1 m from an omnidirectional source, the reverberant sound level may be estimated from Equation (6), where R is room constant, S is room surface area, and $\bar{\alpha}$ is average absorption coefficient.

$$L_{\text{reverb}} = 10\log\left(\frac{4}{R} \div \frac{1}{4\pi}\right) = 10\log\frac{16\pi}{R} = 10\log\frac{16\pi(1-\bar{\alpha})}{S\bar{\alpha}} \tag{6}$$

Values for L_{reverb} are predictable for rooms of defined volume (V), and would typically be larger when volume is smaller. A simpler approximation, neglecting the room's surface area, can be made using absorption, $A = S\bar{\alpha} \approx 24\ln(10)V/cT$, where c is the speed of sound and T is reverberation time (Equation (7)).

$$L_{\text{reverb}} = 10\log\frac{16\pi}{A} \tag{7}$$

For example, a small room with a volume of 50 m^3 and a reverberation time of 0.5 s would have an approximate L_{reverb} value of 4.9 dB; a room with a volume of 1000 m^3 and a reverberation time of 1 s would have an approximate L_{reverb} value of −5.5 dB. More generally, a small room can evidently strongly support a source through reverberation, and the example here has a value of L_{reverb} that is about the same as the incoherent energy sum from a single reflection returning all energy to the source (Equation (5)). However, a large room dilutes the reverberant energy over its volume, so high values of L_{reverb} may not be achievable without excessively long reverberation, and might not be achievable at all, even with excessive reverberation.

These values can be related to voice support using the theoretical model proposed by Pelegrín-García et al. [45]. Voice support (ST_V) is the reflected energy from a mouth reflected to the ears of a head and torso simulator relative to the direct energy from mouth to ears, and has been used as a physical parameter in influential studies of voice regulation due to room acoustics. Theoretically predicted octave band voice support values (125 Hz–4 kHz bands) are calculated following Equation (8). Here, Q^* is the directivity factor of speech in the direction of the floor, d is the transducer height, S_{ref} is the reference surface area (approximately 1 m^2, being the ratio of the product of reference power and characteristic acoustic impedance to the squared reference pressure), ΔL_{HRTF} is the diffuse field head-related transfer function of the ears, and K represents the direct sound level from mouth to ear of a head and torso simulator (see Pelegrín-García et al. [45] for details).

$$ST_{V,\text{oct}} = 10\log\left[\left(\frac{cT_{\text{oct}}}{\ln(10^6)V} - \frac{4}{S} + \frac{Q^*_{\text{oct}}}{4\pi(2d)^2}\right)S_{\text{ref}}\right] + \Delta L_{\text{HRTF,oct}} - K_{\text{oct}} \tag{8}$$

Using the octave-band speech-weighting proposed by Pelegrín-García et al. [45], a small room with a volume of 50 m^3 and a reverberation time of 0.5 s would have an overall speech-weighted ST_V value of -6.5 dB; a room with a volume of 1000 m^3 and a reverberation time of 1 s would have an ST_V value of −15.6 dB (assuming a floor-to-ceiling height of 3 m and a square floor plate). More broadly there is an 11 dB difference between L_{reverb} and speech-weighted ST_V based on evaluation of Equations (6) and (8), with deviations for large rooms and high absorption coefficients (Figure 1). In real rooms, spectral variation in reverberation time, as well as non-diffuse reflections, would be expected to cause further deviations. Figure 1 includes experimental results from real rooms (most of which are described in [46]), which have a 13 dB difference between L_{reverb} (from measured mid-frequency reverberation time T_{20} and room volume) and measured speech-weighted ST_V.

The right axis of Figure 1 shows a model of voice regulation from ST_V, which provides an indication of how increased acoustic support can lead to a more relaxed speaking projection [47]. It is important to bear in mind that the extent of voice regulation depends on the communication scenario; in this case the participants' task was to give a lecture in various real rooms and participants were especially sensitive to the rooms' acoustic support (in conjunction with likely multimodal influences). The question raised in this paper is whether L_{retro} could play a substantial role in providing such acoustic support, partially or largely substituting for L_{reverb}, and potentially leading to more comfortable conditions for speaking.

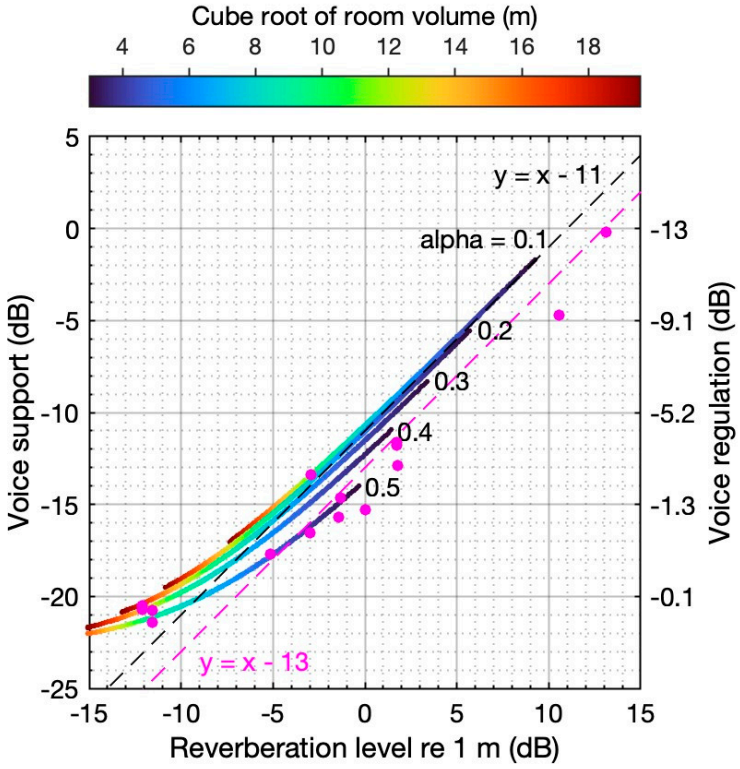

Figure 1. Relationship between L_{reverb} (Equation (6)) and ST_V (Equation (8)) of theoretical diffuse rooms, with characteristic room dimension, $V^{1/3}$, indicated by the colormap. Room volumes range from 27 m^3 to 7500 m^3. A reflective floor in the area around the talker is assumed for theoretical ST_V. Data from real room measurements (using mid-frequency reverberation time and room volume to calculate reverberant level) are shown as magenta points. The right axis gives an example of predicted voice regulation from voice support (from [47]).

1.2. Retroreflectors and Focusing Retroreflectors

Retroreflective array surfaces provide an obvious way of concentrating early reflected sound at the source without knowledge of the source's position. Their effect has been explored in prior studies, albeit in mostly outdoor spaces or in laboratory settings [44,48–52]. However, while retroreflective arrays can achieve a substantial boost in sound returned to the source, more may be needed; for this reason, we consider the potential of focusing retroreflectors.

Acoustic retroreflection can be achieved through passive acoustic devices that provide space-reversal across their face. The three examples in Figure 2 achieve this over reasonably broad spectral and spatial ranges in different ways, each with distinct advantages and disadvantages. The cat's eye and van Atta reflectors have wider acceptance angles than the cube corner reflector but involve more elaborate construction. For example, a cat's eye lens might be created from a gas balloon [53] (e.g., xenon, which has a refractive index close to 2 with respect to air), from an intricate metamaterial (which can have a graded index of refraction, i.e., a Luneburg lens [54]), or even with a flat lens and mirror [55]. The van Atta reflector [56] is an intricate and bulky construction, and its high-frequency response is inherently limited by its spatial physical discretization. The complexities of these devices can lead to acoustic losses, as well as substantial costs. Hence, the cube corner reflector's simplicity has practical appeal in treating large architectural surfaces. Within its narrower acceptance angle, the cube corner reflector's efficiency varies markedly with incidence angle: common designs are most efficient on-axis, but also have local efficiency peaks for full dihedral and single-face specular reflection angles [57].

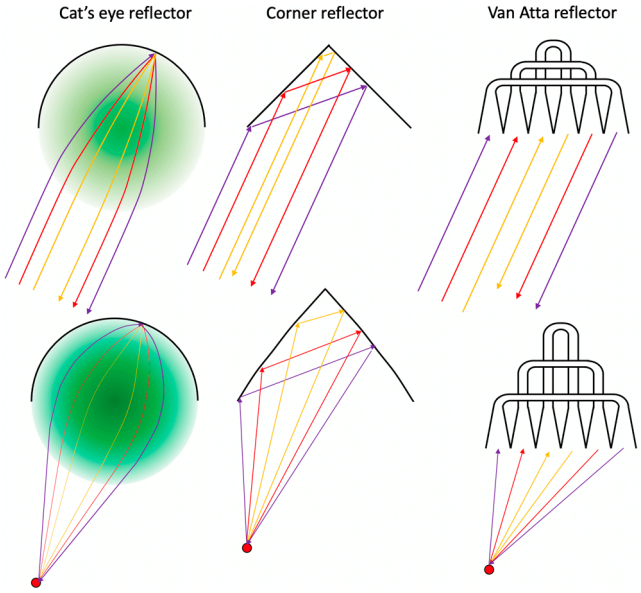

Figure 2. Sketches of some passive acoustic devices that can have reasonably broad spectral and spatial retroreflective performance. The cat's eye reflector is a semicircular or hemispherical mirror with a lens that focuses onto it; the second-order reflection of a dihedral corner reflector, and the third-order reflection of a trihedral cube corner reflector, are retroreflected; the van Atta reflector [56] uses equal-length pipes to spatially reverse the surface. The bottom row illustrates adjustments that could lead to focusing combined with retroreflection: increasing the cat's eye lens' refractive index gradient, curving the corner reflector, and varying the van Atta reflector's pipe lengths.

Each of these devices can be made to focus: the cat's eye reflector can have an increased refractive index lens; the corner reflector can have co-focused parabolic faces (Appendix A); and the van Atta reflector can have pipe lengths increasing towards the center of its face. Alternatively, a converging acoustic lens over the face of any retroreflector can be designed for a focal plane. For a sound source with a spherical wave front, 6 dB is lost from geometric dispersion on the return path from a non-focusing retroreflector to the source, and conceivably more than this 6 dB could be gained from focusing.

Focusing retroreflectors are rarely studied because most applications in optics and radar are far-field, and the retroreflection literature in acoustics is underdeveloped. In acoustics, Cabrera et al. [51] demonstrated an array of four cube corner reflectors (square trihedra), each with two faces optimally warped to enhance retroreflected sound concentration within a few meters. Most of the improved sound concentration of the warped 0.5 m edge-length trihedra was at high frequencies, but a 1 m edge-length version had enhanced effectiveness over a broader frequency band. Inoue et al. [58] describe a focusing single-wavelength infra-red electromagnetic retroreflector, exploiting resonance as part of the retroreflective mechanism. Other studies have examined more general focus adjustments of retroreflectors. Minato et al. [59] describe a diverging cube corner optical retroreflector for spacecraft by very slightly curving the trihedral surfaces. Similarly, Otsubo et al. [60] show how velocity aberration due to the motion of the Earth and Moon can be compensated for by slightly splaying one face of a lunar ranging trihedral retroreflector. Fang et al. [61] describe focus improvements of retroreflectors by lens design for wireless information and power transmission to portable devices.

In room acoustics, a ceiling can have advantages for treatment, partly because substantial treatment can be installed without physically interfering with occupant activities. For focusing retroreflectors, the ceiling has an advantage in that people's heads will mostly be within a known range of heights—indicatively about 1.2 m seated to 1.5 m standing—allowing the selection of a generally advantageous focal length for local over-

head reflectors. Hence, the scenarios examined in this paper could apply well to ceiling treatment, but in some circumstances they might also apply to walls or room dividers.

2. Materials and Methods

The key concept examined in this paper—an array of focusing acoustic retroreflectors—is difficult to approach literally because physical design/fabrication challenges have not been entirely solved. However, idealized retroreflector and focusing retroreflector arrays can be simulated computationally, and this paper uses finite-difference time-domain (FDTD) simulation to do this. It also uses FDTD to simulate reflections from focusing trihedra, which are physically realizable non-ideal cases.

2.1. Ideal Retroreflection from a Ceiling

2.1.1. Discrete Surface Transformations for Ideal Reflections

An ideal acoustic reflector is conceived of as a flat hard surface divided into patches that may undergo transformation between sound incidence and re-emission (reflection). Each patch is divided into numerous elements that are small compared to the shortest wavelength of interest. If no patch transformation occurs (referred to as a simple patch), then the reflection is expected to be specular. Figure 3c illustrates the concept of space-reversal patches, whereby the elements are spatially flipped between incidence and reflection. If patches are sufficiently large, then this should result in ideal retroreflection. In such conditions, each patch's image is projected by the source reflection such that all illuminate the source and the area around it.

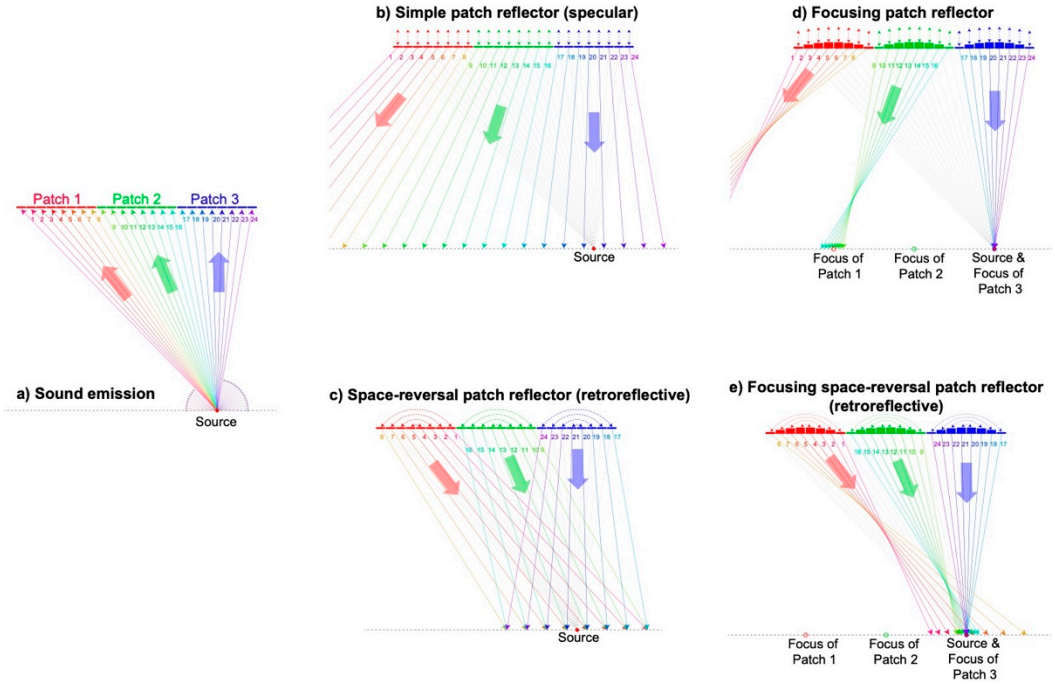

Figure 3. Concepts illustrated by ray analogy in modelling reflections from a flat surface made up of patches, each of which is made up of numerous elements: (**a**) sound is emitted by a source and received by elements; (**b**) if no processing is done, the re-emitted sound from the elements behaves as a specular reflection; (**c**) space-reversal of elements in each patch introduces retroreflection, superimposing the projected images of the patches, with the source at their centres; (**d**) elementwise delays introduce focusing (in this example the source is at the focus of Patch 3); (**e**) the combination of focusing and space-reversal is retroreflective, with a potentially high concentration of reflected rays at and near the source. The ray illustration neglects wave phenomena such as diffraction and interference.

A further step is to introduce focusing for each of the patches. Focusing can be achieved by introducing a delay that is greatest for central elements in each patch. Thus, the elementwise latency of $\Delta\tau = 2d/c$ is introduced, d being the depth of an idealized well to create the appropriate delay. Preliminary experimentation showed that focal points on the source plane aligned with each patch's centroid are effective for retroreflection when combined with space-reversal, including when the source-receiver is not at any patch's focus. While the focus may not be geometrically perfect at such off-focus positions, sound concentration is still achieved by focus-like behavior. The required elementwise latency is calculated from the distance of each element to the patch's focus, r_{focus}, by reference to the maximum such distance for the patch (Equation (9)).

$$\Delta\tau_i = \frac{2(r_{\text{focus,max}} - r_{\text{focus},i})}{c} \tag{9}$$

Note that a minimum latency of $\tau_{\text{min}} = 2\sqrt{2}a/c$ (using the convention of $2a$ for reflector patch width) is required for non-focusing space-reversal square patches for the space-reversal mechanism to function at the speed of sound. Focusing space-reversal patches involve additional elementwise latency, so overall latency is the sum $\tau_i = \tau_{\text{min}} + \Delta\tau_i$.

Two square reflector sizes were evaluated: a 'large' reflector (7.2 × 7.2 m) and a 'small' reflector (2.4 × 2.4 m). The large case was intended to reasonably represent an extensive reflector, with no source-receivers near the edges of the reflector area. Source-receivers were in a 2.4 × 2.4 m square aligned with the reflector's center, so the large reflector's shadow had a 2.4 m margin extending beyond the source-receiver area. The small case represented a local reflector, and had source-receivers over the entire reflector area, up to the edges. Various square patch sizes from 0.3 × 0.3 m up to the full reflector size were evaluated.

2.1.2. Finite-Difference Time-Domain (FDTD) Calculations

The FDTD calculations were carried out in two stages. Firstly, a pulse was emitted from an omnidirectional source in free space, bounded by a perfectly matched layer. The envisaged reflector square was transparent, and entirely populated by receivers. The wave from the source arriving at the receivers was recorded. The wave 1 m from the source was also recorded for reference. Simulations were run for 25 source positions per scenario, with sources mostly within a 2.4 × 2.4 m square area in line with the reflector (one exception was made so that a source could be at the focus of a 3.6 m patch for the large reflector).

In the second stage, the received waves were emitted by hard sources corresponding to the receivers from the first stage, thereby imitating a reflector. Apart from the hard sources, the space was free, and bounded by a perfectly matched layer. Receivers in the second stage were on a plane the same distance from the reflector as the original source, and included the original source. However, only 500 receivers were used in the second stage, and were mostly distributed over a 2.4 × 2.4 m square area in line with the reflector (with the one exception as noted above). All source positions in the first stage were included as receivers in the second stage.

Between the first and second stages, the transformation of square patches (if applicable) within the reflector was carried out as outlined in Section 2.1.1: i.e., space-reversal and/or delay-based focusing.

To manage computational resources, two simulation resolutions were used. For the small reflector, the emitted wave upper cutoff frequency was 11,233 Hz (the cutoff of the 8 kHz octave band), with a sampling rate of 112,330 Hz (10 × cutoff), and a rectilinear inter-element spacing of 5.3 mm. For the large reflector, the emitted wave cutoff frequency was halved, sampling rate was 56,165 Hz, and inter-element spacing was 10.6 mm, to cover frequencies to the upper limit of the 4 kHz octave band. Hence, 206,116 elements were used to represent the small reflector, and 463,761 to represent the large reflector. The speed of sound in simulations was c = 344 ms^{-1}. The time periods for the simulations were sufficient for the receivers to completely capture the incident waves.

FDTD simulation was implemented in C++, interfaced using MATLAB, following the framework proposed by Sheaffer et al. [62]. The 10-element perfectly matched layer design was based on Chern [63]. The simulation was significantly accelerated using GPU parallel computing based on the CUDA toolkit [64].

2.1.3. Calculating Retroflected Energy Levels from Impulse Responses

Retroreflected energy levels (Equation (10)) were calculated from octave-band-filtered impulse responses (125 Hz–4 kHz or 125 Hz–8 kHz).

$$L_{\text{retro,oct}} = 10 \log \left(\frac{\int p_{t,\text{retro,oct}}^2 dt}{\int p_{t,\text{1m,oct}}^2 dt} \right) \tag{10}$$

To provide a single-number result, the octave bands were then weighted using a combination of the ISO 3382-3:2022 omnidirectional speech spectrum and A-weighting (Table 1) [65]. The concept of this weighting is to provide results relevant to long term speech power levels and simplified hearing sensitivity, without any assumptions about the talker's orientation relative to the reflector. The weighting, w_{oct}, over the six or seven octave bands, was applied as per Equation (11). This is referred to as speech-A-weighting in this paper.

$$L_{\text{retro,AS}} = 10 \log \left(\frac{\sum_{\text{oct}=1}^{N} 10^{(L_{\text{retro,oct}} + w_{\text{oct}})/10}}{\sum_{\text{oct}=1}^{N} 10^{w_{\text{oct}}/10}} \right) \tag{11}$$

Table 1. Speech- and A-weighting values in decibels for the seven octave bands spanning 125 Hz–8 kHz. Values are in decibels.

Octave Band	Speech Spectrum [1]	A-Weighting	Speech-A-Weighting [2]
125 Hz	49.9	−16.1	−23.6
250 Hz	54.3	−8.6	−11.7
500 Hz	58.0	−3.2	−2.6
1 kHz	52.0	0.0	−5.4
2 kHz	44.8	1.2	−11.4
4 kHz	38.8	1.0	−17.6
8 kHz	33.5	−1.1	−25.0

[1] Omnidirectional speech sound pressure level at 1 m, from ISO 3382-3:2022 [65]. [2] Combined speech-A-weighting adjusted to energetically sum to 0 dB (w_{oct} in Equation (11)).

Similar calculations were done for receivers that were not collocated with the source.

2.2. Focusing Retroreflectors from Surface Geometric Form

Physically realizable focusing retroreflectors were modeled based on square trihedra, the surfaces of which were parabolically warped. These are referred to as 'parabolic trihedra'. The specifics of the design (Figure 4) are explained in Appendix A. Four configurations were modeled:

- A single 'small' parabolic trihedron with 1 m edge lengths;
- A single 'large' parabolic trihedron with 1.65 m edge lengths;
- An array of seven small parabolic trihedra;
- An array of seven large parabolic trihedra.

With a central source-to-vertex distance of 3.15 m, the small and large single trihedra have the same solid angle as a 1.2 × 1.2 m and a 2.4 × 2.4 m patch at a 2 m distance (0.34 and 1.09 steradians), respectively. The arrays of seven small and large trihedra have solid angles of 1.30 and 3.21 steradians, respectively. By way of comparison, the 2.4 × 2.4 m and 7.2 × 7.2 m square reflectors (Section 2.1.2) have solid angles of 1.09 and 3.52 steradians, respectively, at a 2 m distance.

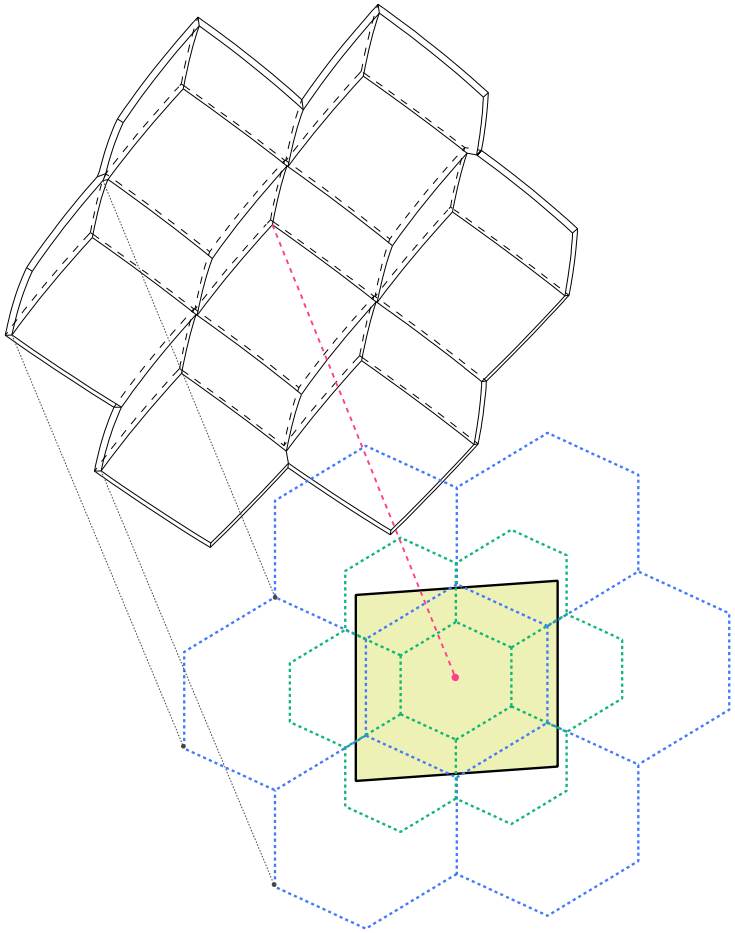

Figure 4. The seven large parabolic trihedron array and its shadow on the source-receiver plane (blue). The shadow of the small array is also shown (green). Single trihedron cases only use the one in the respective array center. Sources are within the yellow area (2.4 × 2.4 m). The red dotted line traces the central source-to-vertex distance, which was extended for clarity.

Reflected energy levels from each configuration were evaluated using FDTD, as described in Section 2.1.2. Twenty-five source positions were in a 2.4 × 2.4 m square offset from the reflector configuration, and receivers were in the same plane. However, the transformation of square patches was not needed here, and a higher sampling rate (144,000 Hz) was used to represent the curved geometry more accurately.

3. Results

3.1. Large Ideal Reflector Array

The following subsections are concerned with various aspects of the sound returned from the 7.2 × 7.2 m ideal reflecting surface, calculated over the 125 Hz to 4 kHz octave band range. To constrain the scope, most attention is given to a surface distance of 2 m, and patch size of 1.2 m (comprehensive results are available at [66]).

3.1.1. Retroreflected Energy Levels

The distributions of speech-A-weighted retroreflected energy levels (L_{retro}) for the 25 source-receivers in a square offset from the large reflector are shown in Figure 5 (boxplots for 2 m and 4 m surface distances) and Figure 6 (energy averages for space-reversed and space-reversed focusing patches, 1.5–4 m surface distances). The 'simple' (neither spatially reversed nor focusing) patch size had no effect, because the patches involve no change. The range of reflected energy for a given surface distance was very small in the simple case for

all tested surface distances. Results deviated by less than 0.1 dB from theory (Equation (3)) for each of the six surface distances.

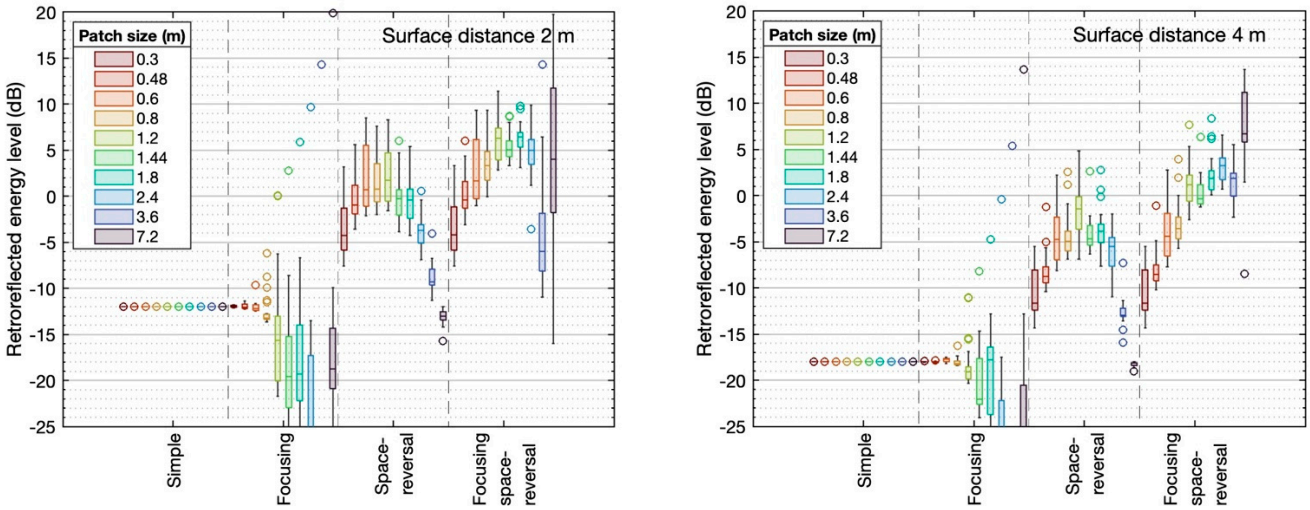

Figure 5. Distribution of retroreflected energy levels for 25 collocated source-receivers. The reflector is a 7.2 × 7.2 m square, and 24 source-receivers are in a 2.4 × 2.4 m square centered on the reflector at (**a**) 2 m or (**b**) 4 m distance. One source-receiver is at the focus of a 3.6 m patch on the same plane, beyond the 2.4 × 2.4 m square. Values are speech-A-weighted.

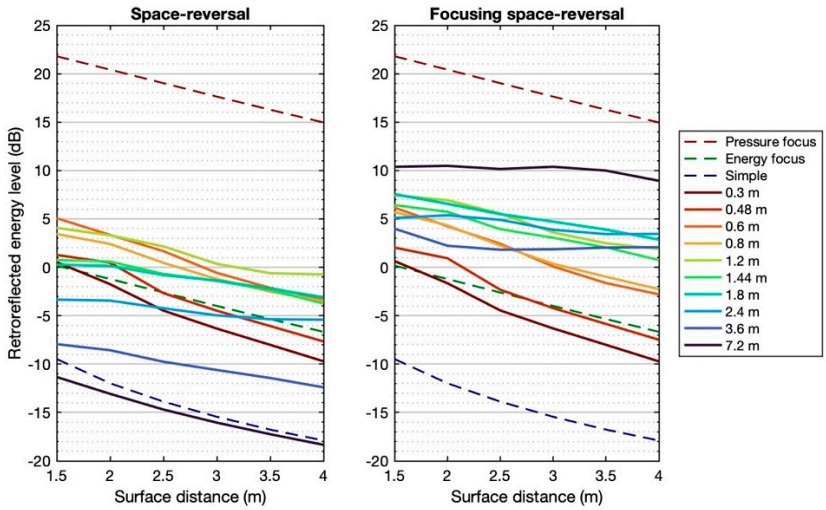

Figure 6. Spatially averaged retroreflected energy levels at collocated source-receivers for space-reversal and focusing space-reversal surface configurations. Twenty-four source-receivers are located within a 2.4 × 2.4 m square offset from the centroid of a 7.2 × 7.2 m reflector, and one is located at the focus of a 3.6 m patch. Distances from source-receiver to reflector are indicated by the *x*-axis. Dashed lines show theoretical expectations (Equations (2), (4) and (5)). Values are speech-A-weighted.

The results for focusing patches were strikingly different. For small patches (e.g., 0.3 m) the patches were too small to have a substantial focusing effect. As the patch size increased, the maximum (at the focus of a patch) increased, but the range of values increased even more dramatically. Hence, the results describe a reflector that introduces a highly variable retroreflected energy level over the source-receiver plane, which does not have an obvious useful application in architectural contexts. The single 7.2 m patch spans the entire reflector, with an extremely large range of values over the 2.4 × 2.4 m source-receiver square. The

maximum value for the single patch was consistently less than theory (Equation (4)), but within 0.7 dB. Note that the bulk of the 3.6 m focusing patch results are very low, partly because the patch's focus is beyond the 2.4 × 2.4 m source-receiver square.

Results for space-reversal patches show increased medians, and relatively small ranges, which is consistent with retroreflection. Retroreflection was most efficient for 0.6 m to 1.2 m patch sizes. The single 7.2 m patch was ineffective in boosting the retroreflected energy, yielding results slightly lower than the simple reflector. The reason for the slightly reduced L_{retro} is that spatial reversal introduces retroreflection at incidence angles larger than 0°.

The focusing space-reversal patches had the most promising retroreflected energy levels. The maximum for the 7.2 m patch was the same as that for the focusing patch without space reversal, which is expected when the source is at the patch focus. However, at a 2 m surface distance the extreme range of single 7.2 m focusing space-reversal values makes it an unlikely design choice; whereas at a 4 m distance the range is less extreme. The subdivided reflector patches provided strong retroreflected energy with a usefully small ranges of values over the source-receiver plane. The optimum patch size (in the 1.2 to 2.4 m range) was larger than for the non-focusing space-reversal cases. Focusing was ineffective for small patch sizes.

The energetically averaged retroreflected energy levels over the 25 collocated source receiver positions are shown in Figure 6 for space-reversal and focusing space-reversal patches. The space-reversal patch reflectors in the range 0.8 m to 1.8 m have mean values consistently greater than would be produced by a simple energy focus (Equation (5)) for a source centered on the reflector. Space-reversal patch sizes in the 0.6 m to 1.2 m range yield the greatest mean retroreflected energy levels.

For the focusing space-reversal cases, the single 7.2 m patch yields mean retroreflected energy levels substantially greater than the smaller patches, with a mean in the vicinity of 10 dB. Apart from the single 7.2 m patch, the focusing space-reversal patch reflectors in the 1.2 m to 1.8 m range yield the greatest mean retroreflected energy levels for the smaller surface distances, for which mean values are often above 5 dB. At the largest surface distance, larger patches (1.8 m and above) are the most effective.

Figure 6 also shows the theoretical values for a simple flat surface (Equation (2)) and a pressure focus (Equation (4)) for a source-receiver centered on the reflector (or an equivalent solid angle spherical cap) at the given distance. All mean results are substantially less than the theoretical coherent pressure focus.

3.1.2. Spatial Distribution of Reflected Energy

The four types of patches had markedly different effects on the spatial distribution of reflected sound. Figure 7 shows results for the 1.2 m patches, which were good performers for both focusing and non-focusing space-reversal configurations. The simple reflector reflected sound quite evenly across the receiver plane, with no sound concentration zones. The focusing patches created strong zones of sound concentration, which were mostly not at the source location. The depicted 2.4 × 2.4 m receiver square aligned with four 1.2 m patches, the natural foci of which were in the center of each quadrant. The non-focusing space-reversal patches usually concentrate sound in the vicinity of the source. The sound field is patterned from the superimposed projections of multiple square reflectors, and in many cases the source position is not at the sound field maximum. On the other hand, in most cases the focusing space-reversal patches have a maximum at or close to the source. The contrast across the receiver square is consistently more than 20 dB for focusing space-reversal patches.

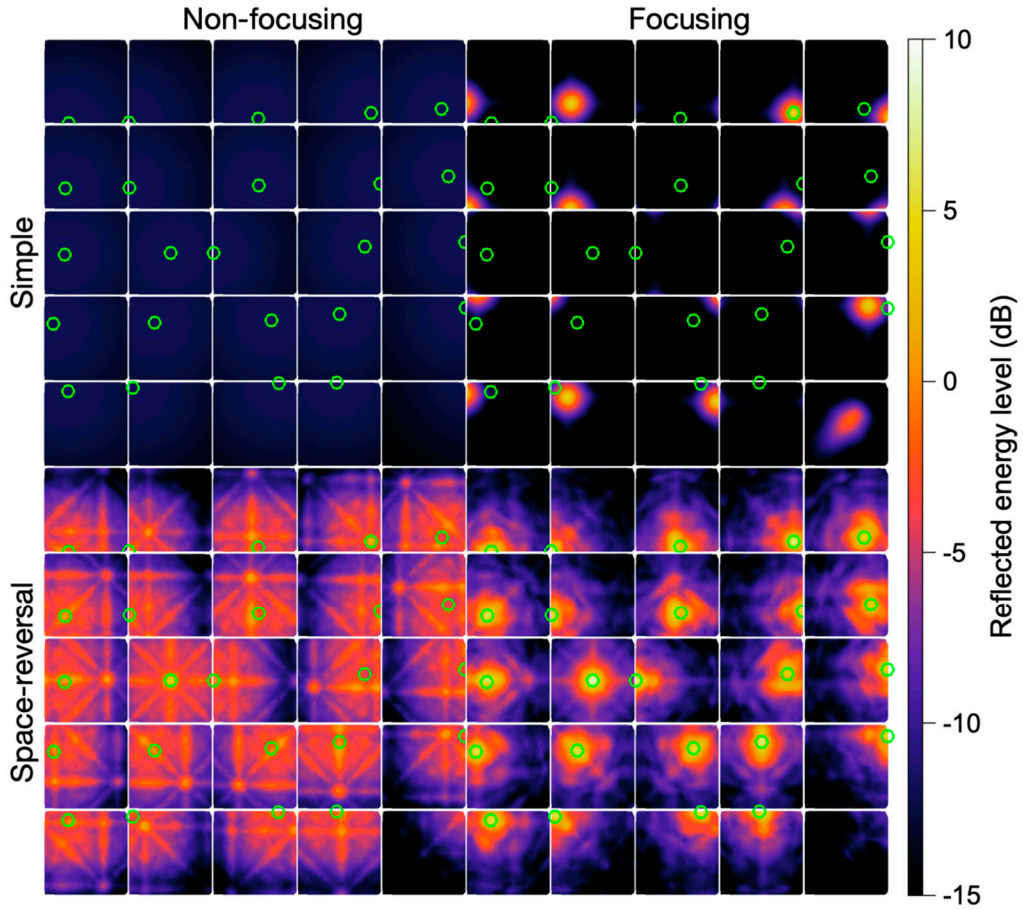

Figure 7. Spatial distribution of reflected energy level over a 2.4 × 2.4 m square for 25 source positions 2 m from the 7.2 × 7.2 m reflector, with 1.2 m patches. The top left quadrant shows the simple reflector; the top right quadrant shows a focusing array; the bottom left quadrant shows the 1.2 m space-reversal array; and the bottom right quadrant shows the focusing space-reversal array. Source locations are indicated by the green circles (the source for the bottom left subplot of each quadrant is outside of the receiver square). Values are speech-A-weighted.

Further results for non-focusing and focusing space-reversal patches are shown in Figure 8 for small (0.6 m) and large (2.4 m) patch sizes. Focusing had little effect on the reflected sound field when the patch size was small, but had a strong effect when the patch size was large. For the non-focusing 2.4 m space-reversal patches, the reflected sound field was not noticeably concentrated at the source, but the reflected energy level is considerably greater than the simple specular case. Of course, it should be borne in mind that the receiver square was the same size as the 2.4 m patches, so the nine projected patch images tend to fill much of the receiver square. By contrast, the focusing 2.4 m space-reversal patches exhibited a strong concentration of reflected energy onto the source.

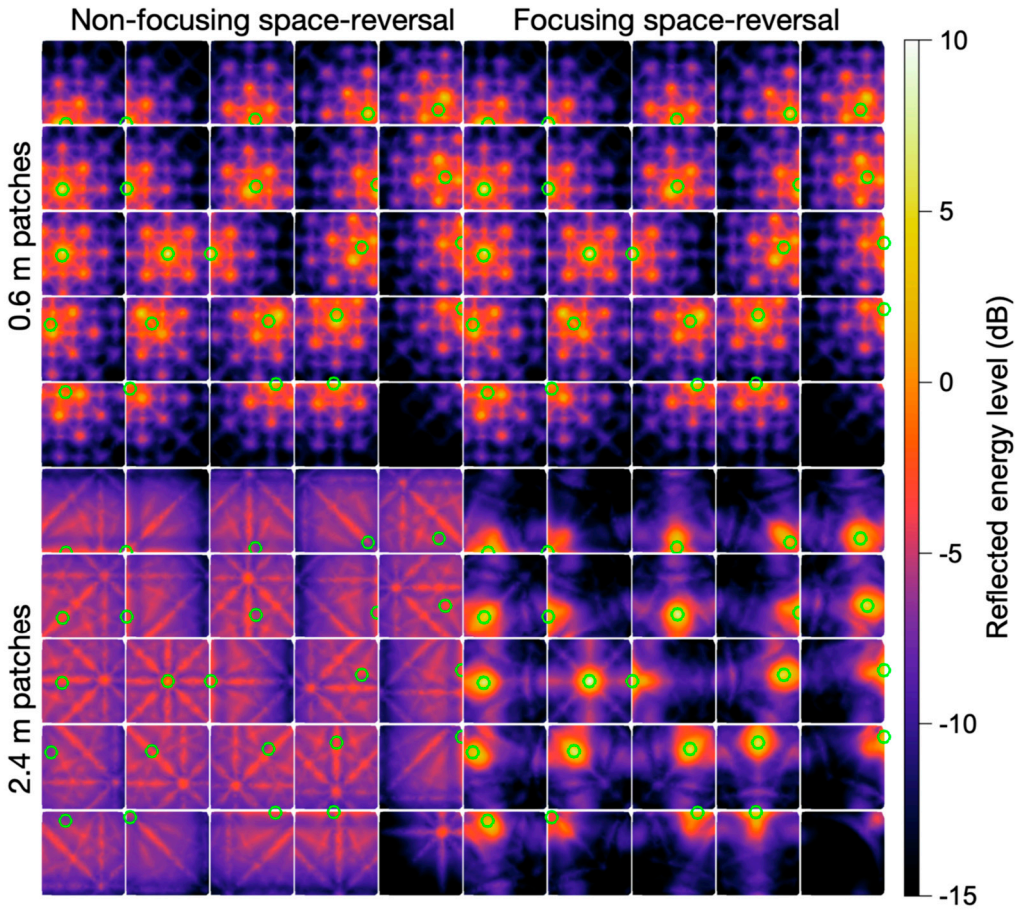

Figure 8. Spatial distribution of reflected energy level over a 2.4 × 2.4 m square for 25 source positions 2 m from the 7.2 × 7.2 m reflector, with space-reversal patches. Small (0.6 m) and large (2.4 m) patch sizes are shown, for non-focusing and focusing space-reversal patches. Source locations are indicated by the green circles (the source for the bottom left subplot of each quadrant is outside of the receiver square). Values are speech-A-weighted.

3.1.3. Spectral Distribution of Retroreflected Energy

The octave band transfer function spectra at collocated source-receivers are influenced by multiple factors, and Figure 9 shows the results for space-reversal and focusing space-reversal patches (2 m surface distance). Mostly the lower limit of the transfer function, seen at low frequencies, was −12 dB which is the same value as the expectation for a simple reflection. Small space-reversal patches presented a 6 dB/octave spectral slope, consistent with expectation from diffraction loss. For 1.2 m patches the diffraction loss slope was only seen in the lower part of the spectrum, and it was not present at all for the 2.4 m patches. Focusing space-reversal patches introduced another frequency-dependent phenomenon, and consequently positive spectral slopes can be seen for all patch sizes in Figure 9b. Focusing made a difference in the 2 kHz and 4 kHz octave bands for the 0.6 m patches; for the bands 500 Hz and above for the 1.2 m patches; and over the entire spectrum for the 2.4 m patches.

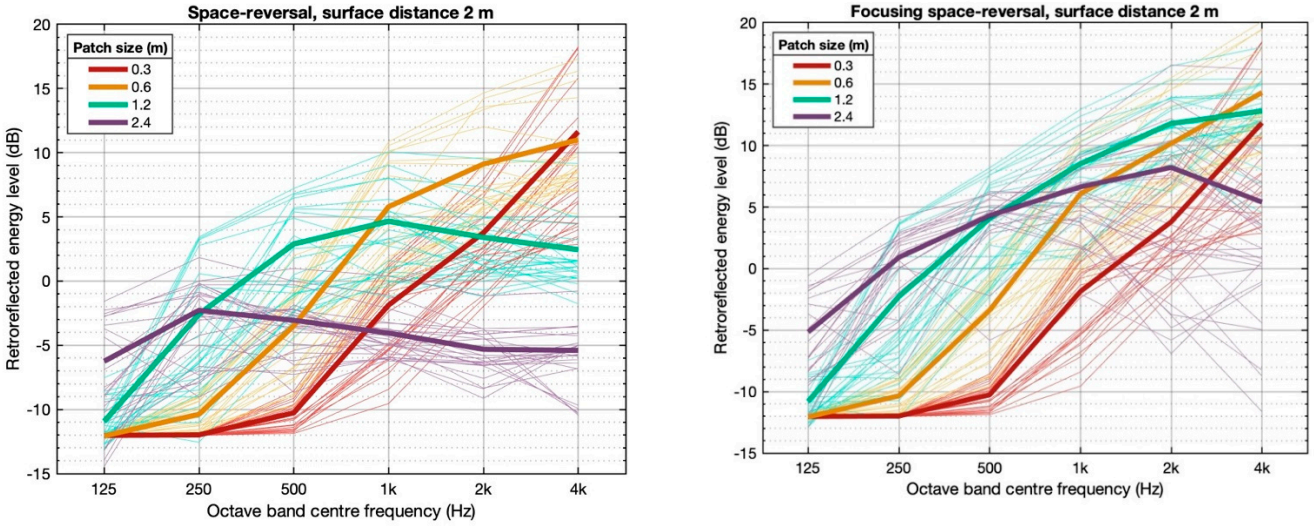

(**a**) (**b**)

Figure 9. Octave-band distribution of retroreflected energy levels for 25 collocated source-receivers (large reflector), showing individual values (thin lines) and energetically averaged values (thick lines): (**a**) space-reversal patches (**b**) focusing space-reversal patches.

Since the 500 Hz and 1 kHz bands have the greatest weight in speech-A-weighting, high transfer function values for those bands are most associated with the high weighted values reported throughout this paper.

3.1.4. Temporal Distribution of Retroreflected Waveforms

The use of distinct patches with focusing and/or space-reversal spreads the energy of the retroreflected waveform over time, because each patch can contribute a distinct reflection to the impulse response. Figure 10 shows two examples of a retroreflected sound envelope and its cumulative sum for the four patch types. The surface distance is 2 m, and patch size is 1.2 m. The additional latency from space-reversal for 1.2 m patches is $\tau_{\text{min}} = 4.9$ ms. To match the other analyses of the large reflector, the impulse responses in Figure 10 were octave-band filtered (6th order 125 Hz–4 kHz center frequencies) and speech-A-weighted before being recombined, and this process spreads the impulse energy in time.

The source-receiver position had little effect on the reflected sound from the simple surface, but had a large effect for the focusing patch. In those cases, the reflected sound event was relatively compact in time. Space-reversal and focusing space-reversal patches yielded extended periods of reflected energy, with contributions from distant patches evident. The source-receiver position did not change the overall temporal spread of reflected energy for those patches. For non-focusing space-reversal surfaces, the cumulative energy sum grew relatively slowly, indicating that numerous patches contribute to the total energy. However, for focusing space-reversal patches, significant energy contributions came from the closest patch and its neighbors, with distant patches making negligible contributions to the total energy.

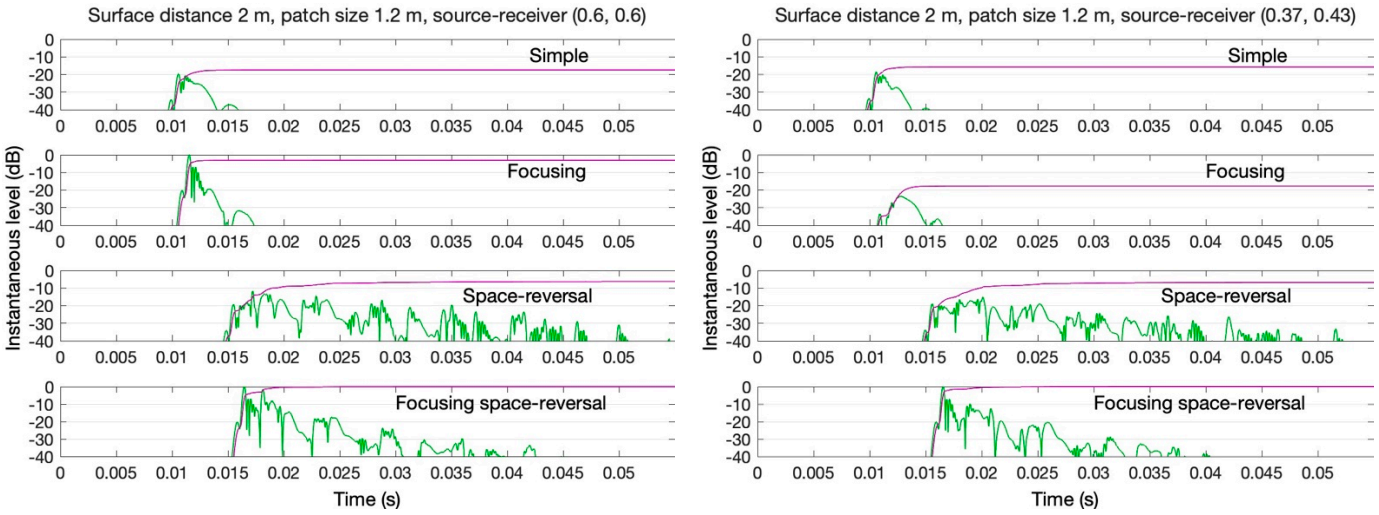

Figure 10. Examples of the time distribution of retroreflected impulse response for the four patch types for the large reflector: (**a**) source-receiver at a patch focus (**b**) source-receiver not at a patch focus. The envelope of the speech-A-weighted impulse responses (absolute value of the Hilbert transform) is shown in green, relative to the maximum peak. The cumulative sum of retroreflected energy is shown in magenta, relative to the greatest maximum value (i.e., focusing space-reversal).

3.2. Small Ideal Reflector Array

The following subsections are concerned with various aspects of the sound returned from the 2.4 × 2.4 m reflecting surface, calculated over the 125 Hz to 8 kHz octave band range.

3.2.1. Retroreflected Energy Levels

The small ideal reflector yielded results similar in pattern to those of the large reflector, but values were generally lower. Figure 11 shows results for the 2 m and 4 m distances for collocated source-receivers. The simple case has a wide range of values because some source-receivers are close to the reflector's edge.

For the 2 m distance, the optimum patch size for space-reversal (0.6 m) was within the optimum range previously observed for the large reflector. While the same could be said for the focusing space-reversal patches, the small reflector size was too small to identify an optimum (the largest patch returned the most sound). Only the focusing space-reversal patches provided cases where the retroreflected energy level was mostly above 0 dB.

For the 4 m distance, retroreflected energy levels were reduced, with no configuration yielding a majority of values above 0 dB. The largest patch size reflected the most sound to the source for both focusing and non-focusing space-reversal patches. Furthermore, the full-surface focusing space-reversal patch yielded a reasonably small range of retroreflected energy levels in this case (unlike the 2 m distance small or large reflector). Although the levels were not high, the median is about 15 dB greater than the simple reflector's maximum at 4 m.

All simulated results were lower than theoretical predictions. Simple patch results from the center of the source-receiver square were on average 0.58 dB less than in theory (Equation (2)), with a maximum deviation of 1 dB over the six reflector distances. For source-receivers at the focus of the 2.4 m focusing patch, levels were on average 0.34 dB less than in theory, with a maximum deviation of 0.4 dB.

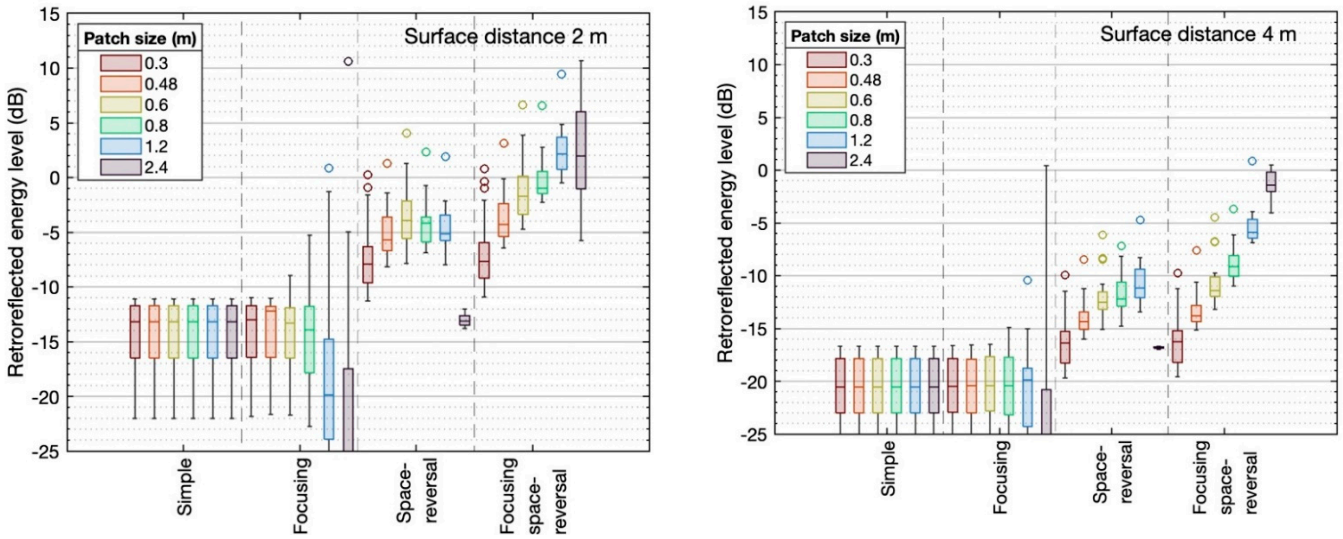

(**a**) (**b**)

Figure 11. Distribution of retroreflected energy levels for 25 collocated source-receivers. The reflector is a 2.4 × 2.4 m square, and 25 source-receivers are in a 2.4 × 2.4 m square offset from the reflector at (**a**) 2 m or (**b**) 4 m distance. Values are speech-A-weighted.

Mean retroreflected energy levels decreased quite consistently with surface distance. For many of the cases in Figure 12, the slope was about the same as the theoretical energy focus slope, suggesting that the retroreflected energy level was mostly related to the surface's solid angle. However, larger focusing space-reversal patches had a gentler slope, especially the single 2.4 m patch. Note that the Equation (2) theoretical flat-square reflector yields a stronger reflection than Equation (5) energy focusing beyond 2 m surface distance because of the surface's relatively small solid angle.

3.2.2. Spatial Distribution of Reflected Energy

The spatial distribution of reflected sound over the receiver plane had some common characteristics with that of the larger reflector. Figure 13 shows results for the four 1.2 m patches (2 m surface distance). The simple patch results show the projection of the square reflector when the source is near the edge. The focusing patches yielded results similar to the large reflector. Non-focusing space-reversal patches yielded simpler patterns of spatial distribution than the large reflector, more obviously concentrating around the source in most cases. The focusing space-reversal array surface yielded the greatest correspondence between sound concentration and source position. Notably, sound concentration on the source even applies to source positions at the edge of the reflector's area for both focusing and non-focusing space-reversal patches.

3.2.3. Spectral Distribution of Retroreflected Energy

The spectral distribution of retroreflected sound from the small reflector differed from that of the large reflector (Figure 14). For space-reversal patches, there was a clear trade-off between the number of patches and the patch size. Sixty-four 0.3 m patches showed a strong high-frequency bias at about 6 dB/octave from the 500 Hz octave band; larger patches saw an optimum frequency range extending to lower frequencies, but reducing the number of patches reduced the retroreflected energy overall. The 2.4 m patch is a special case because it covers the entire reflector. Focusing space-reversal patches yielded a consistently strong high frequency bias either due to diffraction loss (small patches) or focusing (large patches). Compared to the large reflector, the small reflector's octave-band transfer functions were most reduced in the lower part of the spectrum.

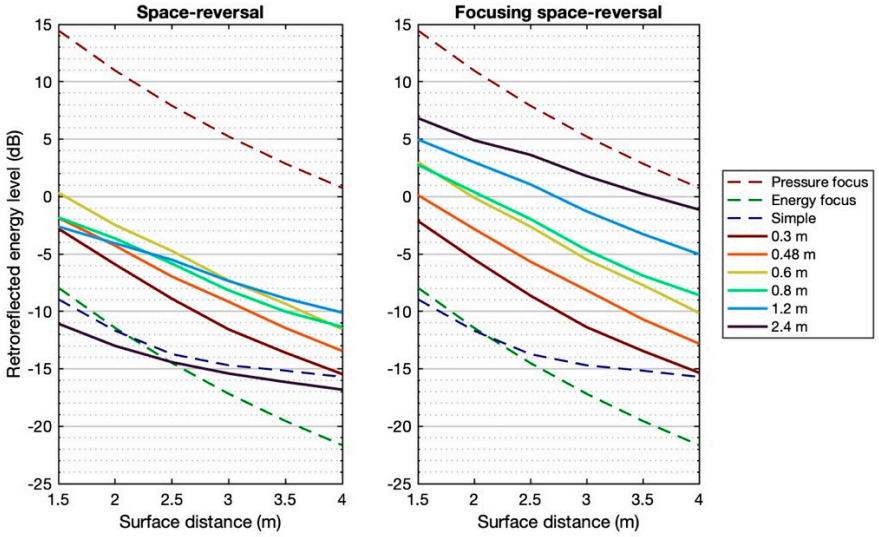

Figure 12. Spatially averaged retroreflected energy levels at collocated source-receivers for space-reversal and focusing space-reversal surface configurations. Twenty-five source-receivers are located within a 2.4 × 2.4 m square offset from a 2.4 × 2.4 m reflector. Distances from source-receiver to reflector are indicated by the *x*-axis. Dashed lines show theoretical expectations. Values are speech-A-weighted.

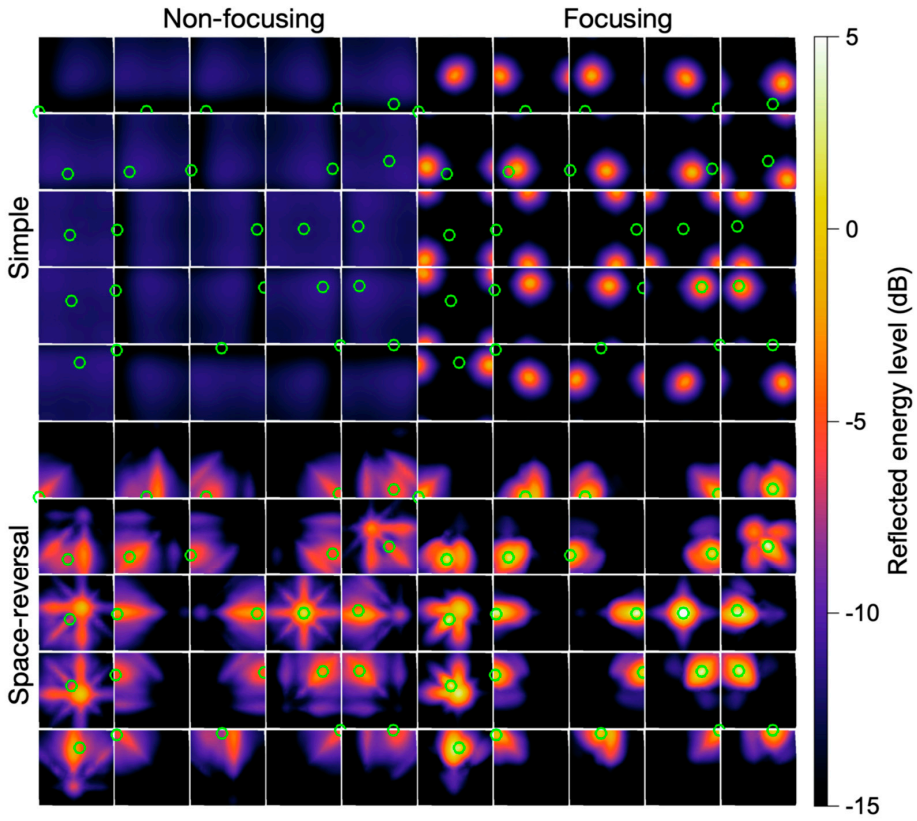

Figure 13. Spatial distribution of reflected energy level over a 2.4 × 2.4 m square for 25 source positions 2 m from the 2.4 × 2.4 m reflector, comprising four 1.2 m patches. The top left quadrant shows the simple reflector; the top right quadrant shows a focusing array; the bottom left quadrant shows the 1.2 m space-reversal array; and the bottom right quadrant shows the focusing space-reversal array. Source locations are indicated by the green circles. Values are speech-A-weighted.

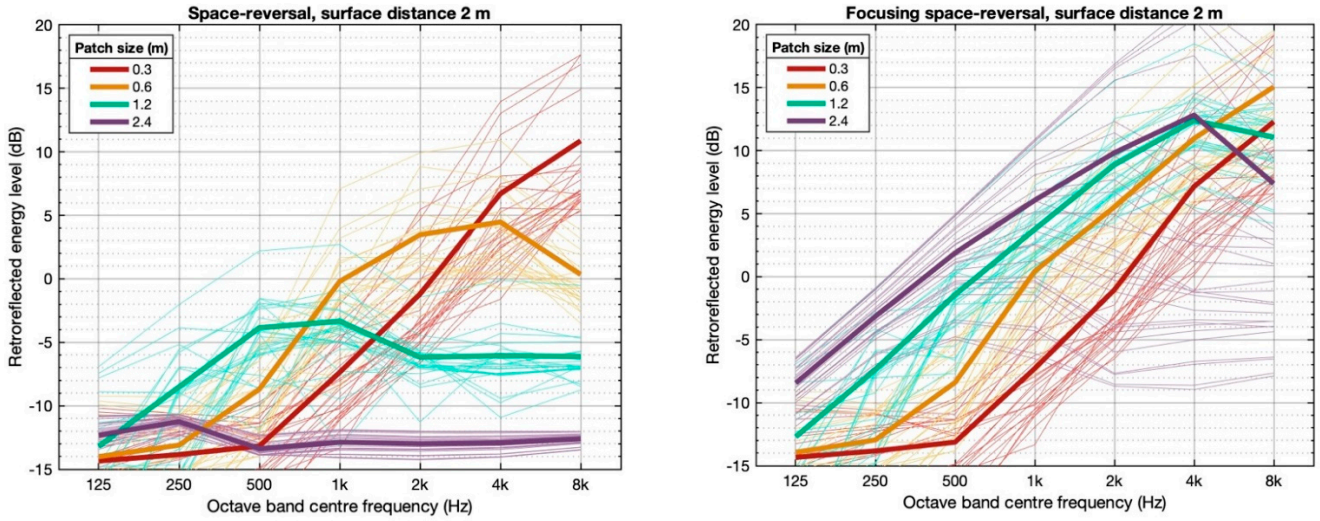

(**a**) (**b**)

Figure 14. Octave-band distribution of retroreflected energy levels for 25 collocated source-receivers (small reflector), showing individual values (thin lines) and energetically averaged values (thick lines): (**a**) space-reversal patches (**b**) focusing space-reversal patches.

3.3. Parabolic-Trihedral Reflectors and Reflector Arrays

3.3.1. Retroreflected Energy Levels

The best overall performance came from the array of seven large parabolic trihedra (Figure 15a), which had both average and median retroreflected energy levels in the vicinity of 5 dB, and a relatively small 8 dB range. These results are similar to the ideal focusing space-reversal patches with widths of 1.2 to 2.4 m for the 7.2 × 7.2 m reflector at 2 m distance (Section 3.1). A single large parabolic trihedron yielded a much larger 20 dB range, including both higher and lower values. It is counterintuitive that increasing the number of trihedra from 1 to 7 would reduce the maximum retroreflected energy level (by 2 dB), but this phenomenon occurs from interference; a similar result is seen for the ideal 2.4 m square patch in Sections 3.1 and 3.2.

Predictably, the single small parabolic trihedron had the least useful results, with retroreflected energy spanning a large range, including many low values. The effect of arraying seven small parabolic trihedra increased the maximum, mean, median, and minimum, and reduced the range. Results for the seven small parabolic trihedra are somewhat similar in distribution to those of the 0.8 m or 1.2 m focusing space-reversal patches for the 2.4 × 2.4 m ideal reflector at a 2 m distance (Section 3.2).

Energetically averaged and median speech-A-weighted results are all much higher than Equation (5)'s theoretical prediction of ideal maximum incoherent summation. The maxima of the single parabolic trihedra are close to Equation (4)'s theoretical ideal focusing prediction, which indicates that the surfaces focus effectively. The single large parabolic trihedron had a maximum 1 dB greater than the theoretical maximum, which might be explained by a contribution from diffraction at the solid edges of the form.

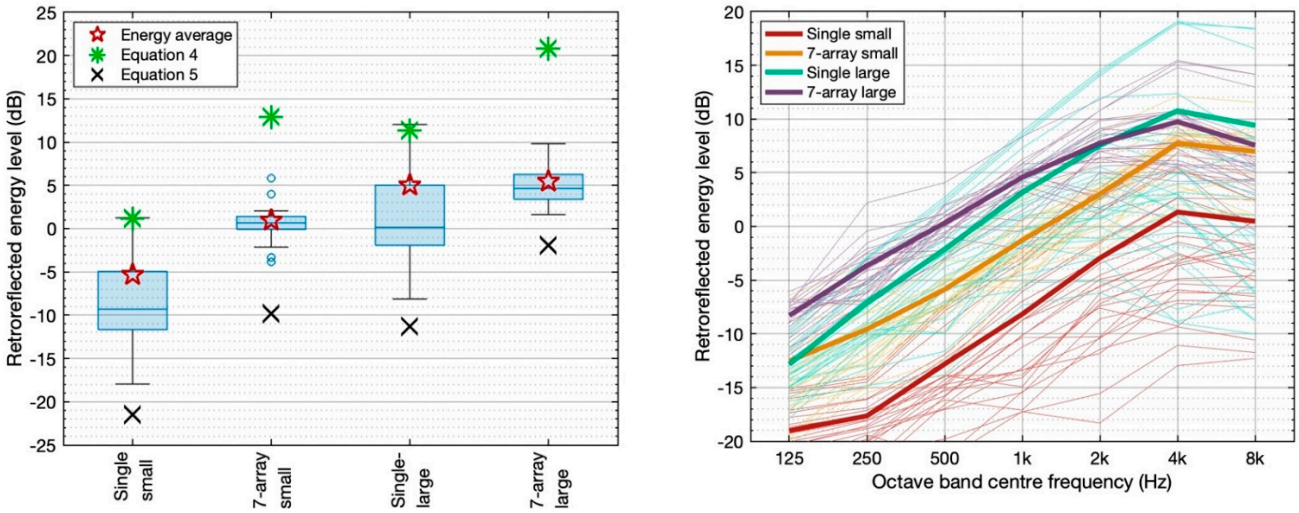

Figure 15. Retroreflected energy levels for 25 collocated source-receivers in a 2.4 × 2.4 m square offset from parabolic trihedral reflector configurations: (**a**) speech-A-weighted distributions, with red star-markers showing energetically averaged values; (**b**) octave band spectral distribution, showing individual values (thin lines) and energetically averaged values (thick lines). Values for Equation (4) (coherent pressure focus) and Equation (5) (energy focus) are calculated from the solid angle of the reflector for a source-receiver aligned with the reflector's centroid.

All configurations yielded positive spectral slopes up to the 4 kHz octave band (Figure 15b). The slope of the seven large parabolic trihedron array was 3.6 dB/octave in the bands up to 4 kHz, less steep than the other configurations. The single large parabolic trihedron yielded the greatest slope (4.7 dB/octave). The small parabolic trihedron configurations both had a slope of 4.1 dB/octave.

3.3.2. Spatial Distribution of Reflected Energy

Spatial maps of reflected energy over a 2.4 × 2.4 m receiver plane demonstrate reflected sound concentration at the source for all parabolic trihedral reflector configurations (Figure 16). Note that the colormap range in the figure is expanded compared to other figures to accommodate the low values of the single small parabolic trihedron. Hexagonal tessellation is evident in the seven-array cases, which typically exhibit a 20 dB range over the displayed 2.4 × 2.4 m receiver plane.

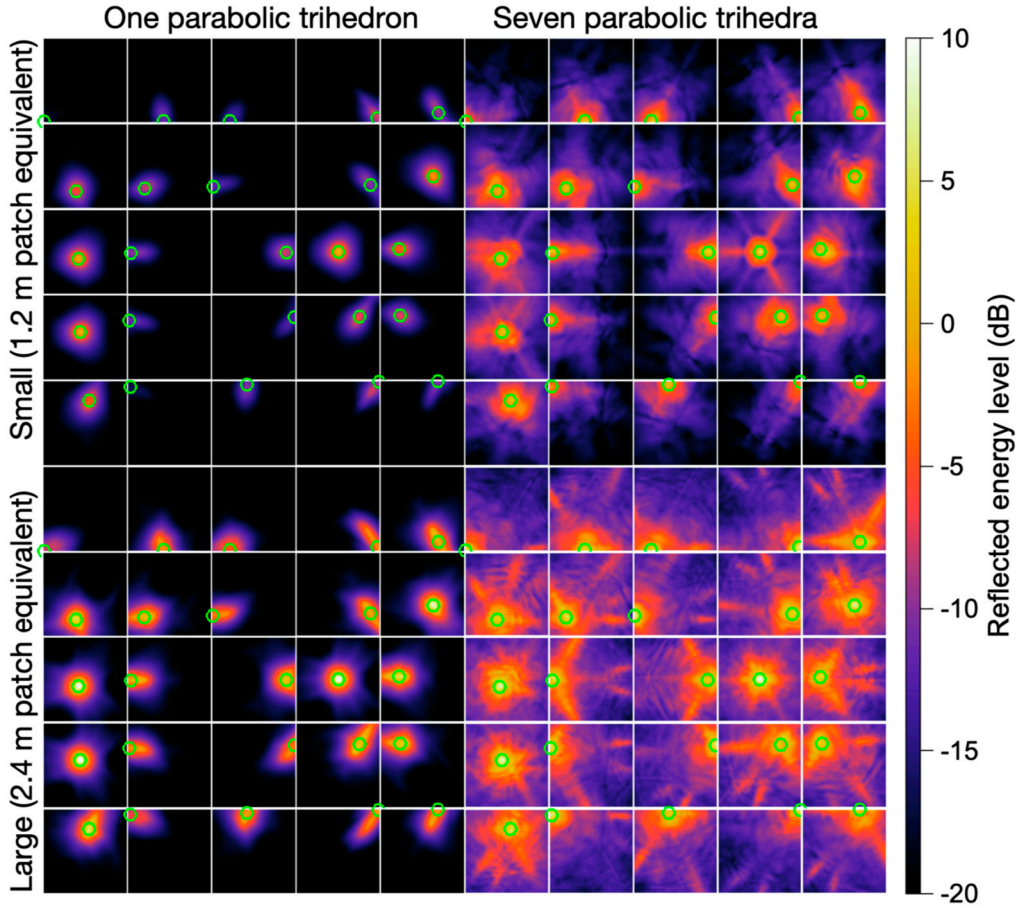

Figure 16. Spatial distribution of reflected energy level over a 2.4 × 2.4 m square for 25 source positions 2 m from reflectors composed of parabolic trihedra (details in the text). Source locations are indicated by the green circles. Values are speech-A-weighted.

4. Discussion

4.1. Discussion of Results

As has been observed in prior studies [44,52], the design of non-focusing acoustic retroreflector arrays involves balancing numerosity with size, considering diffraction loss constraints in relation to a target low frequency roll-off (diffraction loss being size and distance dependent). This is evident in the results of the present study, with optimum patch sizes at various non-focusing retroreflector array distances. Putting aside diffraction, a non-focusing retroreflector array returns superimposed images of the reflector patches that are four times the patch area (Figure 3), so large patches project over a large area rather than concentrating only on the source. However, *focusing* retroreflectors change the array design considerations, because a single patch can concentrate much of the reflected sound at the source. This means that a larger size is not necessarily disadvantageous, as is evident from the results. Multiple focusing retroreflectors yield a more consistent spatial response than a single focusing retroreflector, so there still is an optimum range of sizes for a given source-reflector distance. Even away from the true focus of any patch, a source has a potentially high concentration of sound returned to it from multiple patches, notwithstanding diffraction loss.

Also observed in prior studies has been a high frequency bias in reflections from non-focusing acoustic retroreflector arrays, and the present results indicate that this bias is potentially stronger (or extended) when combined with focusing. Prior studies of real acoustic retroreflector arrays in architectural contexts generally see most effects in high octave bands; 2 kHz and above [44,49,50,52]. Fortunately, the spectrum slope from non-focusing retroreflector diffraction loss applies most to small patches, whereas that from

focusing applies most to large patches in the scenarios tested, so that spectral slopes do not exceed 6 dB/octave.

Although not the main theme of the analyses in this paper, the temporal distribution of reflected sound from non-focusing and focusing retroreflector arrays raises issues for consideration. Assuming that retroreflectors are passive devices, their latency is limited by the speed of sound, which introduces a minimum delay proportional to their size. This is one of the counter-indicators against very large focusing retroreflectors, which could become echo-like if a single strong reflection arrives with excessive delay. Retroreflective arrays introduce clusters of arrivals in the impulse response, which might paradoxically be characterized as a focused diffuse reflection. While focusing retroreflector arrays have less contribution from non-adjacent reflectors than their non-focusing counterparts, they do retain this cluster impulse response characteristic (Figure 10). This desirable characteristic of reflections is linked to the reason why focusing retroreflector arrays return less sound than the theoretical maximum coherent pressure focus (Equation (4)), which can only be achieved if all reflected sound arrives at once.

The simulation results are similar to theoretical predictions. For simple specular and single-patch focusing cases, ideal simulation results are consistently less than the corresponding theoretical expressions in the Introduction, but all within 1 dB. While the theory is limited by simplification, and ideal case simulation has limitations from discretization and error propagation, results concur sufficiently for the context of architectural acoustics. Furthermore, the parabolic trihedral reflector results are credibly close to those of comparable ideal reflector simulations. This study did not include physically fabricated samples, but some previous studies of trihedral retroreflectors have found close correspondence between measurements and FDTD simulations [50]. Experimental verification of near-ideal focusing retroreflector performance could potentially be done using a fabricated reflective surface cut from a sphere, with the source and receiver mutually mirrored around the normal axis of symmetry. This allows space-reversal to be introduced by analysis, even though it does not occur physically, while focusing occurs physically. Another potential quasi-physical method for experimental verification of ideal performance is via an electroacoustic focusing space-reversal mirror (like a time-reversal mirror (e.g., de Rosny et al. [67]), but with different signal processing). However, the performance of real passive retroreflector arrays is a more complex matter, and ideal performance provides a benchmark for real array performance.

Being a conceptual study, there are limitations in translating this study's findings to physical architectural acoustics. The simulations assumed no surface absorption, lossless transmission through air, no scattering from the source or other objects (no other reflective surfaces), an omnidirectional source, time invariance, and so on. The relationship between retroreflected energy level and voice support may differ from that inferred by Figure 1 because of the spatial and spectral distributions of reflections, as well as the limitations of the voice support theoretical model.

4.2. Questions and Challenges

This paper shows that, in principle, it is possible to strongly concentrate reflected sound at arbitrary unknown source positions within an assumed area using focusing retroreflectors. Focusing on its own is an acoustic design hazard (domes have been called an "acoustician's nightmare" [68])—but when combined with space-reversal, focusing could support talkers without relying on reverberation, concentrating reflected sound in the area where it is wanted rather than other areas. However, more scientific research and practical experience with built designs are needed for us to determine whether or not focusing retroreflectors can go from an acoustician's dream to realistic architectural designs. Four important questions are outlined and briefly discussed in the following paragraphs.

Question 1: How can focusing retroreflector arrays be best designed for high acoustic quality in terms of their spectral, spatial and temporal characteristics, especially considering the oral–binaural impulse response? This question includes considerations such as how the

body of a talking listener creates, scatters, and receives the sound field. The mouth and ears are not collocated, and speaking and listening both have directional characteristics. Strong reflections can have positive or negative effects for a talker; delayed auditory feedback can make it very difficult to talk resulting in raised speaking level [69,70], whereas early reflections that are integrated in the auditory system are supportive [71]. The high frequency spectral bias in focusing retroreflection may introduce sound quality issues, although Rapp et al. [72] and the authors' experience with built retroreflective environments [51] provide some indication that this might not be a problem for speech. These multiple issues feed into the question of how focusing retroreflectors should be practically designed for envisaged environments. There are many possible variations in focus design, such as broadband or frequency-selective focusing/defocusing, which may prove to be fruitful in refining spectral and spatial distributions of the reflected sound field. For example, the simulations in this study used ideal retroreflectors focused onto the source-receiver plane, but focusing farther might better balance the contributions of multiple patches.

Question 2: Behaviorally, how do people respond to an acoustic environment strongly supported by focusing retroreflectors? Studies at the time of writing provide only indirect evidence that acoustic support in such an environment will lead to useful voice regulation effects. This is because no space with a large human/speech-scale focusing acoustic retroreflector array has been built anywhere, let alone used for human voice regulation experiments. Indirect indicators of likely voice regulation benefits come from multiple studies using sidetone gain or various room acoustic conditions (not including retroreflection). While these indirect indications are encouraging—given the high voice support values that this study's results suggest—the particular spectral, spatial, temporal and broader contextual factors of focusing retroreflector treatments may affect behavioral response.

Question 3: How should focusing retroreflector arrays be combined with established design techniques such as the use of sound absorption, scattering, and reverberation-based room acoustic design? This question is both practical and theoretical. Design parameter targets and calculation methods may need to be developed and refined for theoretical support of room design incorporating focusing retroreflectors. The hypothesis is that shorter reverberation times combined with greater retroreflected energy can provide improved acoustic conditions for certain types of room, but the theoretical tools to support such design have not been developed.

Question 4: Can space-efficient, acoustically efficient, cost-effective, and visually innocuous focusing retroreflectors be designed for common situations in buildings? Of course it is possible to design architecturally extravagant focusing retroreflector arrays, and perhaps these could have applications in showcase projects. However, in most buildings focusing retroreflector array treatment may be best served by spatially compact, visually unobtrusive, and inexpensive solutions. Hence, practical solutions that meet these criteria and are acoustically efficient need to be developed if this concept is to have widespread deployment.

4.3. Applications

The retroreflected energy levels achieved by the most successful focusing retroreflector array configurations are similar to the reverberant energy levels expected in small reflective rooms. The large ideal reflector yielded several scenarios where mean retroreflected energy level was 5 dB or greater, which in broad terms is comparable to ST_V of -8 dB or greater (Figure 1). Similar results were achieved from the array of seven large parabolic trihedra, demonstrating that these high values are achievable through surface form. If such results are achievable in practical designs, applications could include:

- Didactic rooms (e.g., classrooms) in which the talker's voice could be acoustically supported by focusing retroreflectors, allowing for comfortable speech without reverberant degradation of intelligibility;
- Multi-talker rooms (e.g., offices including activity-based workplaces, eating establishments) where it would be advantageous to return each talker's sound to them to

ameliorate speaking power levels and to reduce unwanted transmission across the space; and

- Outdoor environments, where a wall, canopy or even sculpture-like objects could be shaped to substantially increase acoustic support.

There are probably other potential applications for strong acoustic retroreflectors in architectural environments. Incidental acoustic retroreflectors have been used for robot navigation [73], and designed ones could conceivably contribute to human echolocation. There also may be noise control applications.

5. Conclusions

By generalizing the concept of an acoustic retroreflector as a space-reversal surface, this study was able to investigate ideal acoustic retroreflector array performance for various patch sizes (0.3 m and greater) and distances (1.5 to 4 m). The introduction of delay-based focusing also allowed the systematic investigation of arrays of focusing retroreflectors. Focusing retroreflector arrays were shown to outperform non-focusing counterparts. Physically realizable configurations of parabolic trihedra confirm that results similar to ideal reflector results are possible through the design of passive surfaces.

The study is mostly concerned with speech-A-weighted response because the envisaged applications in buildings are for speech support. For this spectral weighting, findings include:

- The recommended width of individual non-focusing retroreflectors in an array is in the range of 0.6 to 1.2 m (areas 0.36 to 1.44 m^2) for source distances 1.5 to 4 m. An extensive array can achieve mean retroreflected energy levels of -1 dB or more (up to 5 dB), however, a smaller array (a 2.4 m square, with some source-receivers near its edges) is much less effective, especially for larger distances.
- The recommended width of individual focusing retroreflectors in an array is in the range of 1.2 to 2.4 m (areas 1.44 to 5.76 m^2) for source distances 1.5 to 4 m. An extensive array can achieve mean retroreflected energy levels of 3.5 dB or more (up to 7.5 dB). Again, a smaller array returns significantly reduced sound, especially for larger distances.
- While a single large focusing retroreflector can return the most energy to the source for a given solid angle, an array of multiple focusing retroreflectors provides a more even response for a variety of source positions. In an array, focusing retroreflectors adjacent to the nearest one contribute to the retroreflected energy.
- In principle, an extensive focusing retroreflector array can achieve mean speech-A-weighted retroreflected energy levels 15–20 dB greater than an equivalent specularly reflecting surface; and a local (2.4 $\times$ 2.4 m) reflector can achieve retroreflected energy levels more than 10 dB greater than a corresponding specular surface.

These findings are promising indicators of potential solutions to supporting people's speech through architectural surface treatments. However, further research is needed to develop and evaluate practical methods to deploy the concepts introduced by this paper. Envisaged future research by the authors includes the development, characterization, and physical testing of optimal focusing retroreflector array designs for applications such as ceiling treatments. Subsequent human experiments will involve voice-regulation and acoustic qualitative testing of treated environments. Experimental results from this research project will provide the basis for recommendations on improving room acoustics for speech by incorporating high levels of voice support without excessive reverberation.

Author Contributions: Conceptualization, D.C., S.L., J.H. and M.Y.; methodology, D.C., S.L. and J.H.; software, J.H., S.L. and D.C.; validation, D.C. and S.L.; formal analysis, D.C. and S.L.; investigation, D.C. and S.L.; data curation, D.C.; writing—original draft preparation, D.C.; writing—review and editing, D.C., S.L., J.H. and M.Y.; visualization, D.C. and S.L.. All authors have read and agreed to the published version of the manuscript.

Funding: M.Y. was supported by a DFG (German Research Foundation) grant - Project number 503914237.

Institutional Review Board Statement: Not applicable.

Informed Consent Statement: Not applicable.

Data Availability Statement: The data presented in this study are openly available in the Open Science Foundation project "The Potential of Focusing Acoustic Retroreflectors for Architectural Surface Treatment", https://doi.org/10.17605/OSF.IO/4J2BW (accessed on 29 December 2022).

Acknowledgments: Not applicable.

Conflicts of Interest: The authors declare no conflict of interest.

Appendix A. Parabolic Dihedra and Trihedra

The concept behind the parabolic trihedra used as physically realizable focusing retroreflectors can be understood as an extension of the two-dimensional case of parabolic dihedra. A conventional dihedron forms a corner reflector, which is a non-focusing retroreflector in two-dimensional space. A dihedral focusing retroreflector can be formed by extracting segments from two co-focused parabolas, $y = ax^2$ and its vertically mirrored counterpart $y = -ax^2 + 1/(2a)$ (Figure A1). Diverging rays emitted by a source located at the focal point (red, source-to-vertex distance $= 1/(2a)$) are made parallel by the first reflection, and then made to converge by the second, achieving perfect focusing retroreflection. Similarly, soft-focusing retroreflection is achieved for sources elsewhere on or near the Y axis (e.g., blue source and rays).

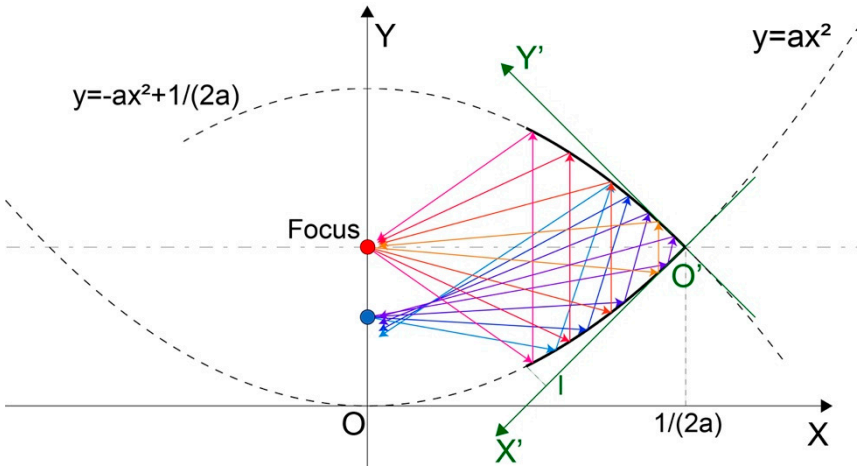

Figure A1. Geometry of co-focused parabolas, which together form a focusing dihedral retroreflector.

For simplicity, $y = ax^2$ in XOY can be represented in X'O'Y' using coordinate transformation rules following Equation (A1).

$$y = \begin{cases} \frac{\sqrt{2}\sqrt{-\sqrt{2}ax+1}-ax+\sqrt{2}}{a} \\ \frac{-\sqrt{2}\sqrt{-\sqrt{2}ax+1}-ax+\sqrt{2}}{a} \end{cases}, \; x \leq \frac{\sqrt{2}}{2a} \tag{A1}$$

The extracted segment can then be written as Equation (A2),

$$y = \left\{ \frac{-\sqrt{2}\sqrt{-\sqrt{2}ax+1}-ax+\sqrt{2}}{a}, \; 0 \leq x \leq l \right. \tag{A2}$$

where l is the edge length of the base dihedron (prior to curvature).

In three dimensions, an exact focusing solution for a trihedron is not known, but an effective solution is achieved by warping the trihedron similarly to the parabolic dihedron. Figure A2 illustrates how each trihedron face can follow a pair of intersecting parabolas.

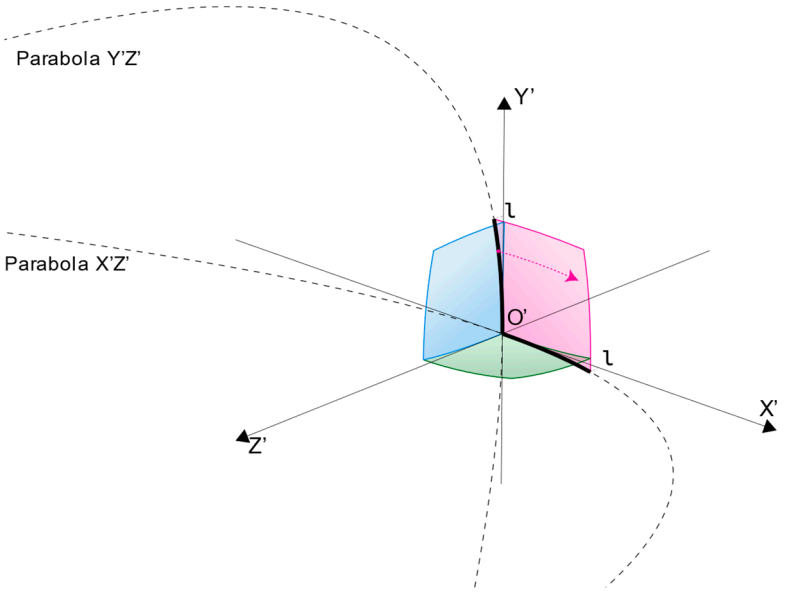

Figure A2. Geometry of a parabolic trihedron, showing how the pink face is formed by two parabolas. The other two faces are formed similarly.

Shown as thick curves in Figure A2, the two segments of intersecting parabolas X′Z′ and Y′Z′ can be, respectively written as Equations (A3) and (A4):

$$z = \begin{cases} \dfrac{-\sqrt{2}\sqrt{-\sqrt{2}ax+1} - ax + \sqrt{2}}{a}, & 0 \le x \le l \end{cases} \tag{A3}$$

$$z = \begin{cases} \dfrac{-\sqrt{2}\sqrt{-\sqrt{2}ay+1} - ay + \sqrt{2}}{a}, & 0 \le y \le l \end{cases} \tag{A4}$$

where l is the edge length of the base trihedron. Then, one segment is swept over the other, i.e., moved along the other to form a double-parabolic surface (shown as the pink surface), the equation of which can be written as Equation (A5):

$$z = \begin{cases} \dfrac{-\sqrt{2}\sqrt{-\sqrt{2}ax+1} - \sqrt{2}\sqrt{-\sqrt{2}ay+1} - ax - ay + 2\sqrt{2}}{a}, 0 \le x, y \le l \end{cases} \tag{A5}$$

Similarly, two other double-parabolic surfaces (the blue and green surfaces) can be formed using parabolas, and these three surfaces together construct a focusing trihedral retroreflector.

Unlike a parabolic dihedron which reflects sound twice and achieves perfect focusing retroreflection for sources at its focal point, a parabolic trihedron reflects sound three times and thus focuses short for sources located at its parabolic focal point. The performance of a focusing trihedron with different source-to-vertex distances was investigated using ray-based simulation, and it was found that the best result, i.e., the highest degree of ray convergence back to the source, is achieved when $1/(2a) = 1.15 \times$ the distance. The parameters of the parabolic trihedra in Section 2.2 were determined using this equation to maximize their performance

Appendix B. Sensitivity to Elementwise Surface Deviation

Real building materials may not be precisely shaped or perfectly smooth, raising the question of how sensitive the reflector configurations are to surface irregularities. In this appendix we consider the effect of local random deviations for the ideal 2.4 × 2.4 m reflector.

Random elementwise delays were introduced to the 2.4 × 2.4 m reflector, for the 1.2 m patch size at a distance of 2 m. The delay is indicated by the additional depth of an idealized well, d_{rand} per element i (Equation (A6)). The additional elementwise depths were determined from a uniform random distribution, spanning the range 0 to δ m. Hence, the mean additional depth is 0.5δ, and the standard deviation 0.29δ, with a 'white' distribution of deviation over the two-dimensional spatial-frequency spectrum (offset by 0.5δ).

$$\Delta\tau_{\text{rand},i} = \frac{2d_{\text{rand},i}}{c}, \quad 0 \le d_{\text{rand},i} \le \delta \tag{A6}$$

Results (Figure A3) indicate that uniformly distributed random delays equivalent to surface roughness with a range of $\delta \le 10$ mm have little effect on the speech-A-weighted retroreflected energy level, but a larger range of random values degrades the retroreflected energy level. The degradation is greatest for focusing space-reversal patches.

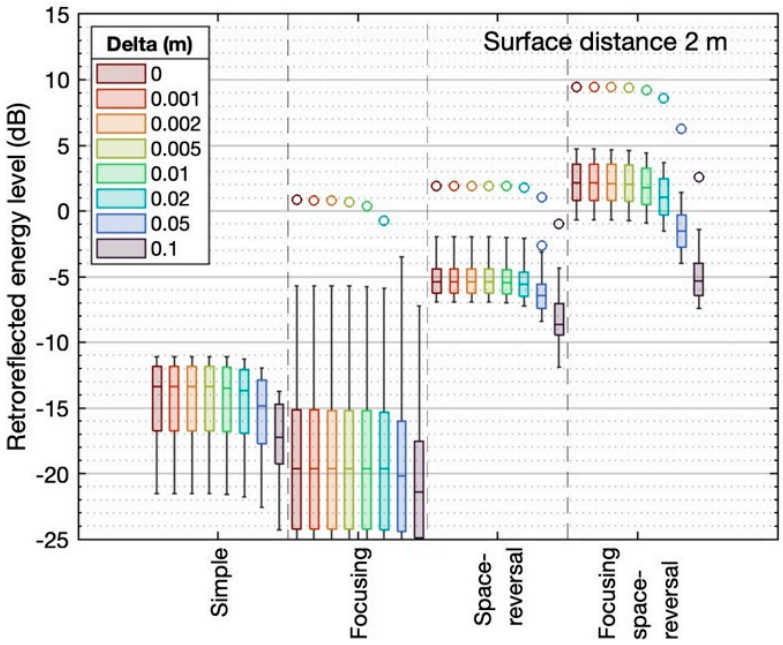

Figure A3. Distribution of retroreflected energy levels for 25 collocated source-receivers for various random elementwise delay ranges, represented by delta (δ). The reflector is a 2.4 × 2.4 m square, and the 25 source-receivers are in a 2.4 × 2.4 m square offset from the reflector at 2 m with a patch size of 1.2 m. Values are speech-A-weighted.

References

1. Gade, A.C. Acoustics for symphony orchestras; status after three decades of experimental research. *Build. Acoust.* **2011**, *18*, 181–206. [CrossRef]
2. Dammerud, J.J.; Barron, M.; Kahle, E. Objective assessment of acoustic conditions for symphony orchestras. *Build. Acoust.* **2011**, *18*, 207–219. [CrossRef]
3. Panton, L.; Yadav, M.; Cabrera, D.; Holloway, D. Chamber musicians' acoustic impressions of auditorium stages: Relation to spatial distribution of early reflections and other parameters. *J. Acoust. Soc. Am.* **2019**, *145*, 3715–3726. [CrossRef] [PubMed]
4. *ISO 3382-1:2009*; Acoustics—Measurement of Room Acoustic Parameters—Part 1: Performance Spaces. International Organization for Standardization, ISO: Geneva, Switzerland, 2009.
5. Brunskog, J.; Gade, A.C.; Bellester, G.P.; Calbo, L.R. Increase in voice level and speaker comfort in lecture rooms. *J. Acoust. Soc. Am.* **2009**, *125*, 2072–2082. [CrossRef] [PubMed]
6. Pelegrín-García, D.; Brunskog, J. Speakers' comfort and voice level variation in classrooms: Laboratory research. *J. Acoust. Soc. Am.* **2012**, *132*, 249–260. [CrossRef]
7. Pelegrín-García, D.; Smits, B.; Brunskog, J.; Jeong, C.-H. Vocal effort with changing talker-to-listener distance in different acoustic environments. *J. Acoust. Soc. Am.* **2011**, *129*, 1981–1990. [CrossRef]
8. Lane, H.; Tranel, B. The Lombard sign and the role of hearing in speech. *J. Speech Hear. Res.* **1971**, *14*, 677–709. [CrossRef]

9. Lane, H.; Tranel, B.; Sisson, C. Regulation of voice communication by sensory dynamics. *J. Acoust. Soc. Am.* **1970**, *47*, 618–624. [CrossRef]
10. Cipriano, M.; Astolfi, A.; Pelegrín-García, D. Combined effect of noise and room acoustics on vocal effort in simulated classrooms. *J. Acoust. Soc. Am.* **2017**, *141*, EL51–EL56. [CrossRef]
11. Lombard, E. Le signe de l'elevation de la voix (The sign of the elevation of the voice). *Ann. Mal. Oreille Larynx Nez Pharynx* **1911**, *37*, 101–119.
12. Lane, H.; Catania, A.C.; Stevens, S.S. Voice level: Autophonic scale, perceived loudness, and effects of sidetone. *J. Acoust. Soc. Am.* **1961**, *33*, 160–167. [CrossRef]
13. Lane, H. Estimates of autophonic level are not estimates of loudness. *J. Acoust. Soc. Am.* **1963**, *35*, 777. [CrossRef]
14. Cooke, M.; Lu, Y. Spectral and temporal changes to speech produced in the presence of energetic and informational maskers. *J. Acoust. Soc. Am.* **2010**, *128*, 2059–2069. [CrossRef] [PubMed]
15. Garnier, M.; Henrich, N.; Dubois, D. Influence of sound immersion and communicative interaction on the Lombard effect. *J. Speech Lang. Hear. Res.* **2010**, *53*, 588–608. [CrossRef] [PubMed]
16. Astolfi, A.; Carullo, A.; Pavese, L.; Puglisi, G.E. Duration of voicing and silence periods of continuous speech in different acoustic environments. *J. Acoust. Soc. Am.* **2015**, *137*, 565–579. [CrossRef]
17. Astolfi, A.; Castellana, A.; Puglisi, G.E.; Fugiglando, U.; Carullo, A. Speech level parameters in very low and excessive reverberation measured with a contact-sensor-based device and a headworn microphone. *J. Acoust. Soc. Am.* **2019**, *145*, 2540–2551. [CrossRef]
18. Therrien, A.S.; Lyons, J.; Balasubramaniam, R. Sensory attenuation of self-produced feedback: The Lombard effect revisited. *PLoS ONE* **2012**, *7*, e49370. [CrossRef]
19. Bottalico, P.; Graetzer, S.; Hunter, E.J. Effects of speech style, room acoustics, and vocal fatigue on vocal effort. *J. Acoust. Soc. Am.* **2016**, *139*, 2870–2879. [CrossRef]
20. Moreno, M.; Calvache, C.; Cantor-Cutiva, L.C. Systematic review of literature on prevalence of vocal fatigue among teachers. *J. Voice* **2022**, *in press*. [CrossRef]
21. Pelegrín-García, D.; Lyberg-Åhlander, V.; Rydell, R.; Brunskog, J.; Lofqvist, A. Influence of classroom acoustics on the voice levels of teachers with and without voice problems: A field study. In Proceedings of the Meetings on Acoustics 160ASA, Cancun, Mexico, 15 November 2010; Volume 11, p. 060001. [CrossRef]
22. Puglisi, G.E.; Astolfi, A.; Cantor Cutiva, L.C.; Carullo, A. Four-day-follow-up study on the voice monitoring of primary school teachers: Relationships with conversational task and classroom acoustics. *J. Acoust. Soc. Am.* **2017**, *141*, 441–452. [CrossRef]
23. Mealings, K. Classroom acoustic conditions: Understanding what is suitable through a review of national and international standards, recommendations, and live classroom measurements. In Proceedings of the Acoustics 2016, Brisbane, Australia, 9–11 November 2016; Available online: http://dspace.nal.gov.au/xmlui/handle/123456789/521 (accessed on 29 December 2022).
24. Pelegrín-García, D.; Brunskog, J.; Rasmussen, B. Speaker-oriented classroom acoustics design guidelines in the context of current regulations in European countries. *Acta Acust. United Acust.* **2014**, *100*, 1073–1089. [CrossRef]
25. Nijs, L.; Saher, K.; den Ouden, D. Effect of room absorption on human vocal output in multitalker situations. *J. Acoust. Soc. Am.* **2008**, *123*, 803–813. [CrossRef] [PubMed]
26. Rindel, J.H. Verbal communication and noise in eating establishments. *Appl. Acoust.* **2010**, *71*, 1156–1161. [CrossRef]
27. Liu, H.; Ma, H.; Wang, C.; Kang, J. Prediction model of crowd noise in large waiting halls. *J. Acoust. Soc. Am.* **2022**, *152*, 2001–2012. [CrossRef]
28. Bottalico, P.; Piper, R.N.; Legner, B. Lombard effect, intelligibility, ambient noise, and willingness to spend time and money in a restaurant amongst older adults. *Sci. Rep.* **2022**, *12*, 6549. [CrossRef]
29. Wang, C.; Kong, X.J.; Yao, S.; Kang, J.; Yuan, J.Y. Crowd noise and vocal power level in large college canteens in China. *Appl. Acoust.* **2021**, *182*, 108242. [CrossRef]
30. Chen, J.; Ma, H. An impact study of acoustic environment on users in large interior spaces. *Build. Acoust.* **2019**, *26*, 139–153. [CrossRef]
31. Wang, C.; Ma, H.; Wu, Y.; Kang, J. Characteristics and prediction of sound level in extra-large spaces. *Appl. Acoust.* **2018**, *134*, 1–7. [CrossRef]
32. Yang, T.T.; Aletta, F.; Kang, J. Sound environments in large public buildings for crowd transit: A systematic review. *Appl. Sci.* **2021**, *11*, 3728. [CrossRef]
33. Haapakangas, A.; Hongisto, V.; Eerola, M.; Kuusisto, T. Distraction distance and perceived disturbance by noise—An analysis of 21 open-plan offices. *J. Acoust. Soc. Am.* **2017**, *141*, 127–136. [CrossRef]
34. Liebl, A.; Assfalg, A.; Schlittmeier, S.J. The effects of speech intelligibility and temporal–spectral variability on performance and annoyance ratings. *Appl. Acoust.* **2016**, *110*, 170–175. [CrossRef]
35. Schlittmeier, S.J.; Liebl, A. The effects of intelligible irrelevant background speech in offices—Cognitive disturbance, annoyance, and solutions. *Facilities* **2015**, *33*, 61–75. [CrossRef]
36. Yadav, M.; Kim, J.; Cabrera, D.; De Dear, R. Auditory distraction in open-plan office environments: The effect of multi-talker acoustics. *Appl. Acoust.* **2017**, *126*, 68–80. [CrossRef]
37. Yadav, M.; Cabrera, D.; Kim, J.; Fels, J.; de Dear, R. Sound in occupied open-plan offices: Objective metrics with a review of historical perspectives. *Appl. Acoust.* **2021**, *177*, 107943. [CrossRef]

38. Yang, H.S.; Kim, M.J.; Kang, J. Acoustic characteristics of outdoor spaces in an apartment complex. *Noise Control. Eng. J.* **2013**, *61*, 1–10. [CrossRef]
39. Yang, H.S.; Kang, J.; Kim, M.J. An experimental study on the acoustic characteristics of outdoor spaces surrounded by multi-residential buildings. *Appl. Acoust.* **2017**, *127*, 147–159. [CrossRef]
40. Almagro-Pastor, J.A.; García-Quesada, R.; Vida-Manzano, J.; Martínez-Irureta, F.J.; Ramos-Ridao, Á.F. The Acoustics of the Palace of Charles V as a Cultural Heritage Concert Hall. *Acoustics* **2022**, *4*, 800–820. [CrossRef]
41. Girón, S.; Álvarez-Corbacho, Á.; Zamarreño, T. Exploring the acoustics of ancient open-air theatres. *Arch. Acoust.* **2020**, *45*, 181–208. [CrossRef]
42. Rindel, J.H. Attenuation of sound reflections due to diffraction. In Proceedings of the Nordic Acoustical Meeting, Aalborg, Denmark, 20–22 August 1986.
43. Vercammen, M. Sound reflections from concave spherical surfaces. Part II: Geometrical acoustics and engineering approach. *Acta Acust. United Acust.* **2010**, *96*, 92–101. [CrossRef]
44. Cabrera, D.; Yadav, M.; Holmes, J.; Fong, O.; Caldwell, H. Incidental acoustic retroreflection from building façades: Three instances in Berkeley, Sydney and Hong Kong. *Build. Environ.* **2020**, *172*, 106733. [CrossRef]
45. Pelegrín-García, D.; Brunskog, J.; Lyberg-Åhlander, V.; Löfqvist, A. Measurement and prediction of voice support and room gain in school classrooms. *J. Acoust. Soc. Am.* **2012**, *131*, 194–204. [CrossRef] [PubMed]
46. Cabrera, D.; Lee, D.; Collins, R.; Hartmann, B.; Martens, W.L.; Sato, H. Variation in oral-binaural room impulse responses for horizontal rotations of a head and torso simulator. *Build. Acoust.* **2011**, *18*, 227–251. [CrossRef]
47. Pelegrín-García, D. Comment on "Increase in voice level and speaker comfort in lecture rooms". [*J. Acoust. Soc. Am.* **2009**, *125*, 2072–2082]. *J. Acoust. Soc. Am.* **2011**, *129*, 1161–1164. [CrossRef] [PubMed]
48. Crawford, F.S. Cube corner retroreflectors for sound waves. *Am. J. Phys.* **1991**, *59*, 176–177. [CrossRef]
49. Cabrera, D.; Holmes, J.; Caldwell, H.; Yadav, M.; Gao, K. An unusual instance of acoustic retroreflection in architecture–Ports 1961 Shanghai flagship store façade. *Appl. Acoust.* **2018**, *138*, 133–146. [CrossRef]
50. Rapp, M.; Cabrera, D.; Lu, S. A polytrihedral dome for acoustic retroreflection, and its application to creative-arts practice-led research. *Appl. Acoust.* **2022**, *195*, 108860. [CrossRef]
51. Cabrera, D.; Holmes, J.; Lu, S.; Rapp, M.; Yadav, M.; Hutchison, O. Voice support from acoustically retroreflective surfaces. In Proceedings of the Euronoise 2021, Madeira, Portugal, 25–27 October 2021.
52. Cabrera, D.; Lu, S.; Holmes, J.; Yadav, M. Sound reflections in Indian stepwells: Modelling acoustically retroreflective architecture. *Acoustics* **2022**, *4*, 227–247. [CrossRef]
53. Thomas, D.C.; Gee, K.L.; Turley, R.S. A balloon lens: Acoustic scattering from a penetrable sphere. *Am. J. Phys.* **2009**, *77*, 197–203. [CrossRef]
54. Fu, Y.; Li, J.; Xie, Y.; Shen, C.; Xu, Y.; Chen, H.; Cummer, S.A. Compact acoustic retroreflector based on a mirrored Luneburg lens. *Phys. Rev. Mater.* **2018**, *2*, 105202. [CrossRef]
55. Song, G.Y.; Cheng, Q.; Cui, T.J.; Jing, Y. Acoustic planar surface retroreflector. *Phys. Rev. Mater.* **2018**, *2*, 065201. [CrossRef]
56. Walther, K. Model experiments with acoustic Van Atta reflectors. *J. Acoust. Soc. Am.* **1962**, *34*, 665–674. [CrossRef]
57. Eckhardt, H.D. Simple model of corner reflector phenomena. *Appl. Optics* **1971**, *10*, 1559–1566. [CrossRef] [PubMed]
58. Inoue, J.; Kusuura, T.; Ueda, R.; Kintaka, K.; Ura, S. Narrowband focusing retroreflector with a thin-film structure. *Appl. Phys. Express* **2021**, *14*, 082003. [CrossRef]
59. Minato, A.; Sugimoto, N.; Sasano, Y. Optical design of cube-corner retroreflectors having curved mirror surfaces. *Appl. Opt.* **1992**, *31*, 6015–6020. [CrossRef] [PubMed]
60. Otsubo, T.; Kunimori, H.; Noda, H.; Hanada, H.; Araki, H.; Katayama, M. Asymmetric dihedral angle offsets for large-size lunar laser ranging retroreflectors. *Earth Planets Space* **2011**, *63*, e13–e16. [CrossRef]
61. Fang, W.; Han, S.; Liu, M.; Liu, Q. Distance and Efficiency Enhancement with Aspherical Retroreflectors for Resonant Beam SWIPT. *IEEE Internet Things J.* **2022**, *9*, 25438–25448. [CrossRef]
62. Sheaffer, J.; van Walstijn, M.; Fazenda, B. Physical and numerical constraints in source modeling for finite difference simulation of room acoustics. *J. Acoust. Soc. Am.* **2014**, *135*, 251–261. [CrossRef] [PubMed]
63. Chern, A. A reflectionless discrete perfectly matched layer. *J. Comp. Phys.* **2019**, *381*, 91–109. [CrossRef]
64. NVIDIA. CUDA Toolkit. 2022. Available online: https://developer.nvidia.com/cuda-toolkit (accessed on 1 May 2022).
65. *ISO 3382-3:2022*; Acoustics—Measurement of Room Acoustic Parameters—Part 3: Open Plan Offices. International Organization for Standardization, ISO: Geneva, Switzerland, 2022.
66. Cabrera, D.; Lu, S.; Holmes, J.; Yadav, M. *The Potential of Focusing Acoustic Retroreflectors for Architectural Surface Treatment*; Open Science Foundation: Charlottesville, Virginia, 2022. [CrossRef]
67. De Rosny, J.; Farin, M.; Fink, M.; Daudet, L.; Prada, C. Array of time reversal transceivers: An application to acoustic focusing. In Proceedings of the 2019 IEEE 20th International Workshop on Signal Processing Advances in Wireless Communications (SPAWC), Cannes, France, 2–5 July 2019; pp. 1–5. [CrossRef]
68. Cox, T.; d'Antonio, P. *Acoustic Absorbers and Diffusers: Theory, Design and Application*, 3rd ed.; CRC Press: Boca Raton, FL, USA, 2017.
69. Black, J.W. The effect of delayed side-tone upon vocal rate and intensity. *J. Speech Hear. Disord.* **1951**, *16*, 56–60. [CrossRef]
70. Howell, P. Changes in voice level caused by several forms of altered feedback in fluent speakers and stutterers. *Lang. Speech* **1990**, *33*, 325–338. [CrossRef]

71. Bradley, J.S.; Sato, H.; Picard, M. On the importance of early reflections for speech in rooms. *J. Acoust. Soc. Am.* **2003**, *113*, 3233–3244. [CrossRef] [PubMed]
72. Rapp, M.; Cabrera, D.; Yadav, M. Effect of voice support level and spectrum on conversational speech. *J. Acoust. Soc. Am.* **2021**, *150*, 2635–2646. [CrossRef] [PubMed]
73. Kuc, R. Recognizing retro-reflectors with an obliquely-oriented multi-point sonar and acoustic flow. *Int. J. Robot. Res.* **2003**, *22*, 129–145. [CrossRef]